Direct modulation of TRPM8 ion channels by rapamycin and analog macrolide immunosuppressants

Balázs István Tóth (ORCID: 0000-0002-4103-4333)[1,2,*,#], Bahar Bazeli (ORCID: 0000-0001-9568-2689)[2,3,*], Annelies Janssens(ORCID: 0000-0002-6735-8248)[2,3], Erika Lisztes (ORCID: 0000-0002-8517-6536)[1], Márk Racskó[1,4], Balázs Kelemen (ORCID: 0000-0002-8994-0132)[1,2], Mihály Herczeg (ORCID: 0000-0002-7938-9789)[5], Tamás Milán Nagy (ORCID: 0000-0003-4766-1992) [6,7], Katalin E. Kövér (ORCID:0000-0001-5020-4456)[6,8], Argha Mitra (ORCID: 0000-0002-5497-1975)[9,10], Attila Borics (ORCID: 0000-0002-6331-3536)[9], Tamás Bíró (ORCID: 0000-0002-3770-6221)[11], Thomas Voets (ORCID: 0000-0001-5526-5821)[2,3,#]

[1]Laboratory of Cellular and Molecular Physiology, Department of Physiology, Faculty of Medicine, University of Debrecen, Debrecen, 4032 Hungary

[2]Laboratory of Ion Channel Research, Department of Cellular and Molecular Medicine, KU Leuven, Leuven, 3001 Belgium

[3]VIB Center for Brain & Disease Research, Leuven, 3001 Belgium

[4]Doctoral School of Molecular Medicine, Faculty of Medicine, University of Debrecen, Debrecen, Hungary

[5]Department of Pharmaceutical Chemistry, University of Debrecen, Debrecen, 4032 Hungary

[6]MTA-DE Molecular Recognition and Interaction Research Group, University of Debrecen, Debrecen, 4032 Hungary

[7]Department of Chemistry, University of Umeå, Umeå, 90187 Sweden

[8]Department of Inorganic and Analytical Chemistry, University of Debrecen, Debrecen, 4032 Hungary

[9]Laboratory of Chemical Biology, Institute of Biochemistry, HUN-REN Biological Research Centre, Szeged, 6726 Hungary

[10]Theoretical Medicine Doctoral School, Faculty of Medicine, University of Szeged, Szeged, 6722 Hungary

[11]Department of Immunology, Faculty of Medicine, University of Debrecen, Debrecen, 4032 Hungary

[*]These authors contributed equally

[#]Corresponding authors:

Balázs István Tóth: toth.istvan@med.unideb.hu, tibalazs@gmail.com
and
Thomas Voets: thomas.voets@kuleuven.be

Keywords: TRPM8, Rapamycin, Electrophysiology, NMR spectroscopy, Neuroscience

Competing Interest Statement:

The authors declare that they have no competing interests.

Funding statement:

The presented work was supported by research grants of the National Research, Development and Innovation Office (grant numbers: 134725 for B.I.T., 134791 for E.L., 137924 for M.H. GINOP-2.3.2-15-2016-00050, GINOP-2.3.3-15-2016-00004, and GINOP-2.3.2–15-2016–00044). B.I.T. was awarded the János Bolyai Research Scholarship of the Hungarian Academy of Sciences. M.R., T.M.N. and B.I.T. were supported by the New National Excellence Program of the Ministry for Innovation and Technology [grant numbers ÚNKP-22-3-I-DE-324 and ÚNKP-23-3-II-DE-430 for M.R., UNKP-22-4-I-DE-87 for T.M.N., and ÚNKP-21-5-DE-491 for B.I.T.] Research in the lab of T.V. is supported by grants from the Research Foundation - Flanders (FWO; G0B9520N), the Research Council of KU Leuven (C2-TRP), the Queen Elisabeth Medical Foundation for Neurosciences and the VIB. The project has received funding from the EU's Horizon 2020 research and innovation program under grant agreement No. 739593.

ABSTRACT

Rapamycin (sirolimus), a macrolide compound isolated from the bacterium *Streptomyces hygroscopicus*, is widely used as oral medication for the prevention of transplant rejection and the treatment of lymphangioleiomyomatosis. It is also incorporated in coronary stent coatings to prevent restenosis and in topical preparations for the treatment of skin disorders. Rapamycin's *in vivo* activities are generally ascribed to its binding to the protein FKBP12, leading to potent inhibition of the mechanistic target of rapamycin kinase (mTOR) by the FKBP12-rapamycin complex. The specific rapamycin-induced interaction between domains from mTOR and FKBP12 is also frequently employed in cell biological research, for rapid chemically-induced protein dimerization strategies. Here we show that rapamycin activates TRPM8, a cation channel expressed in sensory nerve endings that serves as the primary cold sensor in mammals. Using a combination of electrophysiology, Saturation Transfer Triple-Difference (STTD) NMR spectroscopy and molecular docking-based targeted mutagenesis, we demonstrate that rapamycin directly binds to TRPM8. We identify a rapamycin-binding site in the groove between voltage sensor-like domain and the pore domain, distinct from the interaction sites of cooling agents and known TRPM8 agonists menthol and icilin. Related macrolide immunosuppressants act as partial TRPM8 agonists, competing with rapamycin for the same binding site. These findings identify a novel molecular target for rapamycin and provide new insights into the mechanisms of TRPM8 activation, which may assist in the development of therapies targeting this ion channel. Moreover, our findings also indicate that caution is needed when using molecular approaches based on rapamycin-induced dimerization to study ion channel regulation.

INTRODUCTION

TRPM8, a member of the Transient receptor potential (TRP) superfamily of cation channels, has been extensively studied in the context of sensory perception and thermoregulation (Iftinca & Altier, 2020; Kashio & Tominaga, 2022; Vriens et al., 2014). It is highly expressed in a subset of somatosensory neurons, where it acts as the principal molecular detector of decreases in temperature (Bautista et al., 2007; Colburn et al., 2007; Dhaka et al., 2007; McKemy et al., 2002; Peier et al., 2002). TRPM8-deficient mice have pronounced deficits in their response to cool and warm temperatures, do not exhibit cold-induced analgesia and also fail to detect mild warming of the skin (Bautista et al., 2007; Colburn et al., 2007; Dhaka et al., 2007; Paricio-Montesinos et al., 2020). In addition, TRPM8 expression is increased in various malignancies, making it a potential target or biomarker for cancer treatments (Ochoa et al., 2023).

Interestingly, TRPM8 is not only activated by cooling, but also by natural or synthetic cooling agents such as menthol or icilin (McKemy et al., 2002; Peier et al., 2002; Voets et al., 2004). Whereas the conformational changes that lead to cold-induced activation of TRPM8 remain largely elusive, the binding sites of menthol analogs and icilin have been resolved in high detail, based on site-directed mutagenesis studies and high-resolution cryo-EM structures (Bandell et al., 2006; Diver et al., 2019; Voets et al., 2007; Xu et al., 2020; Yin et al., 2019; Yin et al., 2018; Yin et al., 2022). These studies reveal that menthol binds in the cavity between the four alfa-helices of the voltage sensor-like domain (S1-S4), at a position halfway the membrane, where it interacts with residues in S2 and S4 (Xu et al., 2020; Yin et al., 2018). Icilin binds in the same cavity, but slightly closer to the cytosolic side of the membrane, in a binding mechanism that is potentiated by cytosolic calcium (Diver et al., 2019; Zhao et al., 2022). Furthermore, activity of TRPM8 is tightly regulated by the membrane lipid phosphatidylinositol-4,5-bisphosphate (PIP_2), which binds to an

interfacial cavity formed by the outside surface of S4, S5 and several cytosolic domains (Diver et al., 2019; Rohacs et al., 2005; Yin et al., 2019).

Rapamycin is a chemical compound isolated from the bacterium *Streptomyces hygroscopicus*, which was first discovered in a soil sample on Easter Island (Rapa Nui) (Abraham & Wiederrecht, 1996). Initially described as an antifungal agent (Vezina et al., 1975), it was later found to possess potent immunosuppressive properties (Abraham & Wiederrecht, 1996). Subsequent research has uncovered its diverse therapeutic potential, ranging from its use in preventing organ transplant rejection and coronary stent restenosis, to the treatment of lymphangioleiomyomatosis, skin disorders, cancer and age-related diseases (Abraham & Wiederrecht, 1996; Ali et al., 2022; McCormack et al., 2011; Morice et al., 2002; Selvarani et al., 2021; Swarbrick et al., 2021). The various biological and therapeutic effects of rapamycin are primarily attributed to inhibition of mechanistic target of rapamycin kinase (mTOR). Rapamycin binds to the protein FKBP12, leading to an inhibitory interaction of the FKBP12-rapamycin complex with the FRB (FKBP12-rapamycin binding) domain of mTOR (Abraham & Wiederrecht, 1996). The ability of rapamycin and rapamycin analogs to rapidly and efficiently bring FKBP12 and the FRB-domain in close contact has also been successfully engineered for the rapid chemical dimerization and translocation of signaling enzymes or receptors (Muthuswamy et al., 1999), including (TRP) ion channels (Suh et al., 2006; Varnai et al., 2006).

While performing experiments involving rapamycin-induced membrane translocation of a phospholipid phosphatase, we serendipitously discovered that rapamycin by itself potently activates TRPM8, both in TRPM8-expressing HEK cells and in mouse somatosensory neurons. Using whole-cell and inside-out patch-clamp recordings and Saturation Transfer Triple-Difference (STTD) NMR spectroscopy, we demonstrate that channel activation is caused by direct binding of

rapamycin to TRPM8, rather than via an effect on mTOR activity. Based on site-directed mutagenesis guided by molecular docking, we provide evidence for a rapamycin-interaction site in the groove between S4 and S5, distinct from the known interaction sites for menthol or icilin. We also show that related macrolides such as the immunosuppressant everolimus act as partial TRPM8 agonists, and compete with rapamycin for the same binding site. Our results identify TRPM8 as a novel molecular target for rapamycin, and provide new insights into the mechanisms of TRPM8 activation, which may assist in the development of drugs targeting this ion channel. Finally, our results imply that direct activation of TRPM8 may need to be taken into account when using rapamycin-based dimerization approaches to study cellular processes *in vitro* and *in vivo*.

RESULTS

Rapamycin activates TRPM8

When performing Fura-2-based intracellular Ca^{2+} concentration ($[Ca^{2+}]_i$) measurements in HEK293 cells stably expressing human TRPM8 channels (HEK-M8 cells), we observed that rapamycin (10 µM) caused a robust increase in $[Ca^{2+}]_i$, comparable in amplitude to the response evoked by the prototypical TRPM8 agonist menthol at a concentration of 50 µM (**Figure 1A**). Responses to both rapamycin and menthol were fully inhibited by the specific TRPM8 antagonist AMTB N-(3-aminopropyl)-2-[(3-methylphenyl) methoxy] -N-(2-thienylmethyl) benzamide hydrochloride; 2 µM) (Lashinger et al., 2008) (**Figure 1A**). The effect of rapamycin was concentration-dependent, with saturating responses at concentrations ≥10 µM and an EC_{50} value of 3.8 ± 2.0 µM (**Figure 1B**). Similar results were obtained using a 96-well plate-based assay, where we obtained an EC_{50} value of 6.0 ± 0.3 µM at room temperature, which shifted to of 10.1 ± 0.2 µM

at 37 °C (**Figure S1**). Likewise, in whole-cell patch-clamp measurements on HEK-M8 cells at room temperature, rapamycin (10 µM) evoked robust TRPM8 currents, which rapidly returned to baseline upon washout of rapamycin and were fully inhibited by AMTB (2 µM; **Figure 1C**). Half-maximal activation of whole-cell currents at +120 mV was obtained at a rapamycin concentration of 4.5 ± 1.8 µM (**Figure 1D**). Importantly, menthol and rapamycin did not evoke any detectable calcium signal or current increase in non-transfected HEK293 cells (**Figure S2** and **Figure 3C**).

Next, we tested other TRP channels involved in chemo- and thermosensation (Bamps et al., 2021) for their sensitivity to rapamycin (**Figure S3**). We did not observe any sizeable current responses to 30 µM rapamycin in HEK293 cells expressing TRPA1, TRPV1 or TRPM3, whereas large currents were measured in response to their respective agonists allyl isothiocyanate (AITC; 373±173 pA/pF at +120 mV; N=5), capsaicin (1733±677 pA/pF at +120 mV; N=4) and pregnenolone sulfate (PS; 270±71 pA/pF at +120 mV; N=5), respectively.

TRPM8 is expressed in a small subpopulation (5-10%) of somatosensory neurons, where it plays a central role in detection of cool and warm temperature (Bautista et al., 2007; Colburn et al., 2007; Dhaka et al., 2007; McKemy et al., 2002; Paricio-Montesinos et al., 2020; Peier et al., 2002). To evaluate whether rapamycin activates TRPM8 in these neurons, we performed Fura-2-based calcium imaging experiments on somatosensory neurons isolated from the dorsal root and trigeminal ganglia (DRG and TG) of wild type (*Trpm8*$^{+/+}$) and *Trpm8*$^{-/-}$ mice (**Figure 1E**). In wild type neurons, approximately 10% of DRG and TG neurons showed a robust calcium response to rapamycin (10 µM). The large majority (95%) of these rapamycin-responsive neurons also responded to menthol (50 µM). Importantly, responses to rapamycin were largely eliminated in DRG and TG neurons from *Trpm8*$^{-/-}$ animals, indicating that TRPM8 mediates rapamycin responses in sensory neurons (**Figure 1E,F**).

Notably, a subset (~7%) of both *Trpm8*$^{+/+}$ and *Trpm8*$^{-/-}$ neurons responded to menthol but not to rapamycin (Figure 1F). These findings are in line with earlier studies demonstrating that menthol acts as an agonist of not only TRPM8 but also TRPA1 (Karashima et al., 2007; Xiao et al., 2008). In agreement herewith, we found that 92 ± 7% of the rapamycin-insensitive menthol-responsive neurons were also activated by the TRPA1 agonist cinnamaldehyde. Moreover, in experiments using the TRPM8 antagonist AMTB, we found that 2 µM AMTB fully inhibited the calcium responses to menthol and rapamycin in rapamycin-responsive *Trpm8*$^{+/+}$ neurons, whereas menthol responses in rapamycin-insensitive neurons were not inhibited by AMTB (**Figure S2**). Taken together, these findings indicate that rapamycin selectively activates TRPM8-positive sensory neurons, whereas menthol is less selective, exciting both TRPM8-positive and TRPA1-positive neurons.

Taken together, these data show that rapamycin activates TRPM8 in a heterologous expression system and in sensory neurons, and indicate that rapamycin is a more selective tool than menthol to identify TRPM8-positive sensory neurons.

Rapamycin is an agonist ligand directly binding to TRPM8

We initially considered the possibility that the rapamycin-induced activation of TRPM8 in both HEK293 cells and sensory neurons could occur downstream of its effects on mTOR. However, the rapid onset and reversibility of rapamycin's effect on TRPM8 currents, and the observation that low micromolar concentrations of rapamycin were required to induce detectable current activation (compared to the nanomolar concentrations of rapamycin required for mTOR inhibition) (Abraham & Wiederrecht, 1996; Varnai et al., 2006) spoke against an mTOR-dependent effect. Notably, rapamycin also activated TRPM8 when applied to the cytoplasmic surface of

excised inside-out patches (**Figure 2A**), indicating that it acts on TRPM8 in a membrane-delimited manner. Based on these observations we examined whether rapamycin could exert an agonistic action on TRPM8 via direct binding of the compound to the channel protein.

To test a direct molecular interaction between rapamycin and TRPM8, and to obtain insights into the parts of the rapamycin molecule involved in the interaction, we developed the Saturation Transfer Triple-Difference NMR (STTD-NMR) method. (**Figure 2B-E**). This new approach allowed us to obtain a clean ^{1}H-STTD NMR spectrum, eliminating interference from any non-specific interactions present in complex cellular systems. The basic principle of the classical, one-dimensional saturation transfer difference ^{1}H NMR (1D STD-NMR) is that resonances are saturated by selective irradiation, and this saturation spreads over the whole protein molecule and its bound ligands via spin diffusion (Meyer & Peters, 2003). The signal attenuation of ligand ^{1}H resonances upon binding is evident in the saturation transfer difference (STD) spectrum, which is obtained by subtraction of two spectra, one recorded with and the other without the saturation of protein resonances. We calculated the difference of STD spectra (double-difference STD, STDD) (Claasen et al., 2005), one recorded on a cellular sample with rapamycin added (sample 1, STD-1 in **Figure 2B,C**) and the other without rapamycin (sample 2, STD-2 in **Figure 2B,C)**. The resulting double-difference spectrum (STDD-1 in **Figure 2C**) reports both TRPM8 specific and non-specific binding interactions of rapamycin. To remove the STD signals arising from non-specific interactions of rapamycin, we recorded two more STD spectra on cells lacking TRPM8 expression (naïve HEK293 cells), namely in the presence (sample 3, STD-3) and absence (sample 4, STD-4) of rapamycin, yielding the second double-difference (STDD-2) spectrum (**Figure 2C)**. Finally, the difference of STDD-1 and STDD-2 spectra yielded the triple-difference spectrum (STTD), which is free of interfering signals arising from any non-specific interactions (**Figure 2C)**. To address the

effect of the inherent variability of cellular samples on peak heights, STD effects were normalized based on the comparison of independent ^{1}H experiments (Figure S5). Three STTD replicates were computed, unambiguously confirming direct binding to TRPM8 in two datasets (Figure S6A,B). The signals assigned in the STTD spectra (numbered according to the schematic structure of rapamycin; **Figure 2D)** unveil the rapamycin H atoms that correspond to the binding epitopes of the molecule to TRPM8 (**Figure 2E**). Taken together, these findings indicate that rapamycin binds to TRPM8, acting as a direct channel agonist independently of mTOR.

In earlier work, we have classified TRPM8 agonists into two types based on their effect on the channel's gating kinetics (Janssens et al., 2016). According to this classification, Type I agonists such as menthol induce a slowing of the gating kinetics, which is most prominently observed as slowly deactivating tail currents following repolarization, whereas Type II agonists such as AITC cause an acceleration of the kinetics of channel activation upon depolarization, with little or no effect on the kinetics of deactivating tail currents. These differences in kinetics can be explained by a gating model where type I agonist cause a relative stabilization of the open state, whereas type II agonist rather destabilize the closed state (Janssens et al., 2016). Whole-cell current recordings in HEK-M8 cells revealed a pronounced effect of rapamycin on the kinetics of current relaxation in response to voltage steps (see e.g. **Figure 1C; Figure S7**). In particular, rapamycin caused a concentration-dependent slowing of the time course of voltage-dependent activation and deactivation, resulting in long-lasting tail currents upon repolarization from a strongly depolarizing voltage step to +120 mV, and these effects were more pronounced than for menthol (**Figure S7**). Overall, these characteristics classify rapamycin as a type I agonist, stabilizing the channel's open conformations. Notably, rapamycin and menthol had a synergistic effect on

channel gating: application of menthol (50 µM) in the continued presence of rapamycin (10 µM) caused a further slowing down of channel deactivation (**Figure S8**).

Rapamycin binds to a unique binding site on TRPM8

Site-directed mutagenesis studies and high-resolution cryo-EM structures have delineated binding sites for several TRPM8 ligands, including agonists such as icilin, AITC, cryosim-3 and the menthol analog WS-12, as well as antagonists such as AMTB or TC-I 2014 (Bandell et al., 2006; Diver et al., 2019; Voets et al., 2007; Yin et al., 2019; Yin et al., 2018; Yin et al., 2022). These compounds all bind in the cavity between the four alfa-helices of the voltage sensor-like domain (S1-S4), with the exception of the type II agonist AITC, which binds outside the voltage sensor-like domain at a site between S3 and the S4-S5 linker (Yin et al., 2022).

Since rapamycin, like menthol, acts as a type I agonist, and both compounds contain a substituted cyclohexyl moiety, we initially examined the possibility that rapamycin would interact with the menthol-binding site. However, considering the much larger size of rapamycin (molecular weight of 914.2 g/mol) compared to agonists such as menthol, WS-12 or cryosim-3 (molecular weights of 154.3, 260.4 and 289.4 g/mol, respectively), binding of rapamycin in the relatively narrow cavity in the voltage sensor-like domain appeared unlikely. In agreement with this notion, initial experiments revealed that mutations in the menthol binding site that strongly reduce responses to menthol, icilin, Cooling Agent 10, WS-3 or cryosim-3 (Y745H and R842H) (Bandell et al., 2006; Voets et al., 2007; Malkia et al., 2009; Beccari et al., 2017; Plaza-Cayon et al., 2022; Yin et al., 2022; Palchevskyi et al., 2023) did not affect the channel's sensitivity to rapamycin (see **Figure 3**). Therefore, we hypothesized that rapamycin interacts at a different ligand binding site on TRPM8.

To identify potential rapamycin interaction sites, we performed blind, multistep dockings of rapamycin to a model of the human TRPM8 channel based on a cryo-EM structure of mouse TRPM8. Initial pilot dockings revealed several potential rapamycin interaction sites, either at the bottom of the voltage sensor-like domain or in the groove between the voltage sensor-like domain and the pore region (**Figure S9**). Based on these initial results, we made a series of point mutations at strategic residues in these potential rapamycin interaction sites, and used Fura-2-based $[Ca^{2+}]_i$ measurements to test these mutants for their responses to menthol (50 µM) and rapamycin (10 µM; **Figure 3A-C**). All mutant channels yielded robust calcium responses to at least one of the two agonists, indicating that they expressed as functional channels (**Figure 3C**). Wild type and most mutants showed maximal responses ($\Delta[Ca^{2+}]_i$) to at least one of the agonists of >1 µM. One exception was mutant F847A, which did not respond to menthol but showed a consistent but relatively small ($\Delta[Ca^{2+}]_i \approx 200$ nM) to rapamycin (Figure 3C and Figure S10).

To assess potential changes in sensitivity to rapamycin or menthol, we calculated the rapamycin response ratio, defined as the calcium response to rapamycin over the sum of the calcium responses to rapamycin and menthol ($\Delta[Ca^{2+}]_{i,rapamycin}/(\Delta[Ca^{2+}]_{i,rapamycin} + \Delta[Ca^{2+}]_{i,menthol})$). As such, mutants that respond to rapamycin but fully lack a response to menthol have a response ratio of 1, while mutants that respond to menthol but fail to respond to rapamycin have a response ratio of 0. For the wild type channel, which robustly responds to both agonists, this analysis yielded a response ratio of 0.59 ± 0.02 (**Figure 3B**).

Several mutants yielded a significantly higher response ratio compared to wild type, indicating reduced menthol sensitivity. These included the previously described mutants Y745H and R842H (Bandell et al., 2006; Voets et al., 2007), which show robust responses to rapamycin but no responses to menthol (response ratios >0.95; **Figure 3A,B**). These residues, located in the

middle of S1 and S4 respectively, point towards the center of the cavity within the voltage sensor-like domain, where they interact with ligands such as cryosim-3 and the menthol analog WS-12. Mutants R851Q and V849M, located at the cytosolic entrance to the cavity within the voltage sensor-like domain, also show a significantly reduced menthol response combined with a robust rapamycin response (response ratios of 0.77 ± 0.03, and 0.98 ± 0.02, respectively; **Figure 3A,B**). The results from these mutations are fully in line with the notion that menthol activates TRPM8 by binding in the middle of the cavity within the voltage sensor-like domain, and that mutations in the binding site or at the entrance of the cavity affect menthol activation. The observation that rapamycin activation is not noticeably affected in all these mutants confirms that the rapamycin and menthol binding sites are separate, and also argue against a potential rapamycin binding site at the lower part of the voltage sensor-like domain.

Oppositely, we identified four mutants with a significantly lower rapamycin response ratio compared to wild type (response ratios <0.3), indicating reduced rapamycin sensitivity. These include D796A (located in the S2-S3 linker), D802A and G805A (located in S3), and Q861A (located in the S5 pore helix; **Figure 3A,B**)). The strongly reduced sensitivity of these mutants to rapamycin was confirmed in whole-cell patch-clamp recordings, revealing robust current responses to menthol but very limited responses to rapamycin (**Figure 3D,E**). These results further confirm that rapamycin binds directly to the TRPM8 channel, and are in agreement with a model where rapamycin binds in the groove between the voltage sensor-like domain and the pore region. These results and the publication of the cryo-EM structure of the mouse TRPM8 during our experiments prompted the further refinement of dockings, resulting in the rapamycin binding site illustrated in **Figure 4** and **Figure S11** (the pdb-file of the model is available via https://zenodo.org/records/14535771). In this model, rapamycin interacts with residues from a

single subunit. Note that this proposed mode of interaction also largely aligns with the results from the 1H-STTD NMR study, with several of the H atoms that show saturation transfer are effectively in close contact with the channel protein (**Figure S12**).

Mutants D802A and G805A mutations were originally identified due to their ability to reduce icilin-induced activation of TRPM8 (Chuang et al., 2004). Interestingly, structural studies indicated that these residues are not directly involved in binding icilin. Instead, D802 is involved in calcium binding, which strongly potentiates activation of TRPM8 by icilin, while the flexibility invoked by a glycine at position 805 allows enlargement of the VSLD cavity to accommodate the hydroxyphenyl moiety of icilin (Yin et al., 2019). We therefore tested whether rapamycin activation is also modulated by intracellular calcium, by using UV flash-induced release of caged Ca^{2+} during whole-cell current recordings (Mahieu et al., 2010). In these experiments, a 1-ms UV flash was applied during a 800-ms voltage step to + 80 mV, either in the absence of ligand or in the presence of rapamycin (10 µM) or icilin (10 µM). The UV flash caused a rapid increase in intracellular Ca^{2+}, as indicated by the change in Fura-FF fluorescence ratio (Figure 5A). In line with our earlier work (Mahieu et al., 2010), at low cytosolic calcium icilin evokes a sizable current response, which is robustly potentiated of inward and outward currents in the presence of icilin (**Figure 5A-D**). In contrast, currents recorded in the absence of ligand or in the presence of rapamycin were not directly affected by flash-induced calcium uncaging (**Figure 5A-D**). These results demonstrate that rapamycin activation of TRPM8 is not calcium-dependent, and indicate that the reduced rapamycin sensitivity of the D802A mutant is unrelated to this residue's involvement in Ca^{2+} binding.

Effect of rapamycin analogs on TRPM8

According to the proposed binding mode (**Figure 4**), the substituted cyclohexane ring (*trans*-2-methoxycyclohexan-1-ol) of rapamycin is tightly involved in the interaction with TRPM8. In particular, the model predicts a hydrogen bond formed between Q861 and the hydroxyl group on the cyclohexane ring (i.e. on carbon 40 in the rapamycin structure). A number of rapamycin analogs (also known as rapalogs (Lamming et al., 2013)) have been developed as immunosuppressants, in which the hydroxyl group on the cyclohexane ring has been substituted by other functional groups. When tested using Fura-2-based calcium imaging, we found that everolimus, zotarolimus, ridaforolimus and temsirolimus were much less effective than rapamycin in activating TRPM8, with amplitudes that were <10% of that to rapamycin at a concentration of 10 µM (**Figure 6A,B**). The efficacy order was rapamycin >> zotarolimus > ridaforolimus > everolimus > temsirolimus. These results reveal the importance of the substituted cyclohexane ring, and in particular the hydroxyl group on carbon 40, for the activation of TRPM8 by rapamycin.

The calcineurin inhibitors FK506 (tacrolimus) and its structural analog ascomycin contain the same substituted cyclohexane ring (*trans*-2-methoxycyclohexan-1-ol)) as rapamycin, but have a different, smaller macrolactam ring than rapamycin and the rapalogs (**Figure 6A**). Confirming earlier research (Arcas et al., 2019), we found that FK506 evoked robust calcium responses in HEK-M8 cells, albeit less potently than rapamycin (**Figure 6B**). We also measured substantial responses to ascomycin, which were intermediate between were the responses to FK506 and to the most effective rapalog zotarolimus (**Figure 6B**). Pimecrolimus, a derivative of ascomycin in which a chloride substitutes for the corresponding hydroxyl group on the cyclohexane ring did not evoke any detectable calcium response (**Figure 6A,B**). Taken together, these findings demonstrate that

rapamycin is the most effective of the tested macrolides, and illustrate the importance of the hydroxyl group at position 40 on the cyclohexane ring of rapamycin for activating TRPM8.

To investigate whether the substituted cyclohexane ring of rapamycin by itself is sufficient to evoke TRPM8 activation, we synthetized and tested *trans*-2-methoxycyclohexan-1-ol (2-metoxy-CHol). However, we could not detect any TRPM8 responses to 2-metoxy-CHol at concentrations up to 100 µM (**Figure 6A,B**), indicating that the 2-metoxy-CHol moiety is indispensable but insufficient for the activation of TRPM8.

These findings raised the question whether the 2-metoxy-CHol moiety is essential for the binding of the macrolides to TRPM8, or rather affects the ability of the compounds to modulate the gating of TRPM8 following binding. To address this, we performed *in silico* dockings with everolimus, a close structural analog of rapamycin, in which the hydroxyl group on the cyclohexene ring is substituted by a 2-hydroxyethyl moiety. These revealed that everolimus can bind in the same region of TRPM8 as rapamycin, albeit with reduced binding energy (**Figure S13**). In particular, the docking indicated that substituting the hydroxyl group for the 2-hydroxyethyl moiety prevented the formation of a hydrogen bond with the amide of Q861 (**Figure S13**). If everolimus can indeed occupy the rapamycin binding site on TRPM8, without strongly activating the channel, the prediction would be that everolimus reduces the effect of rapamycin by competing for the same binding site. This was indeed confirmed in calcium imaging experiments showing that preincubation with 10 µM everolimus, a concentration which by itself does not evoke a substantial calcium signal, significantly inhibited the response to 10 µM rapamycin (**Figure 6C,E**). In contrast, 10 µM everolimus was without any effect on the response to 50 µM menthol (**Figure 6D,E**). Taken together, these findings indicate that macrolide analogs such as everolimus compete with rapamycin for the same binding site but with strongly reduced potency to activate

the channel. The lack of effect on channel activation by menthol further confirms that the rapamycin and menthol binding sites are spatially separate and independent.

DISCUSSION

Our study demonstrates that, in addition to its well-established inhibitory effect on the mTOR signaling pathway (Abraham & Wiederrecht, 1996; Lamming et al., 2013), rapamycin acts as an agonist of the ion channel TRPM8. Several lines of evidence indicate that the agonistic effect of rapamycin involves a direct interaction with the channel, rather than an indirect effect involving intracellular signaling pathways such as mTOR. First, we found that rapamycin rapidly and reversibly activates TRPM8 currents, not only in the whole-cell mode but also in inside-out patches, indicating a membrane-limited mode of action. Second, we developed STTD NMR methodology, which not only allowed us to demonstrate a direct molecular interaction between rapamycin and TRPM8, but also to identify moieties on rapamycin that interact with the channel. Finally, site-directed mutagenesis steered by molecular docking of rapamycin onto TRPM8 revealed residues that strongly reduce channel activation by rapamycin, while leaving responses to other stimuli intact. Although we cannot exclude that some of these mutations may have an allosteric effect on rapamycin-induced channel gating, the cumulative results are consistent with a model where rapamycin binds in the groove between the voltage sensor-like domain and the pore domain, at a site distinct from the interaction sites of well-studied TRPM8 agonists menthol and icilin.

The effect of rapamycin on TRPM8 occurs at low micromolar concentrations, which contrast to the low nanomolar concentrations required to inhibit mTOR signaling (Abraham & Wiederrecht, 1996; Varnai et al., 2006). Plasma concentrations of rapamycin in patients on

systemic drug regimens following organ transplantation or for the treatment of lymphangioleiomyomatosis or cancer rarely exceed 100 nM (Jimeno et al., 2008; Trepanier et al., 1998), rendering it unlikely that substantial rapamycin-induced TRPM8 activation would occur in these subjects. However, rapamycin is also used topically for the treatment of skin diseases, with the use of creams or ointments containing millimolar concentrations of rapamycin. For instance, a 0.2% rapamycin gel (corresponding to approximately 2 mM) has been approved by the FDA for the treatment of facial angiofibromas in patients with tuberous sclerosis complex, and formulations up to 1% have shown efficacy in preclinical and clinical studies for this and other skin disorders, including psoriasis and oral lichen planus (Aitken et al., 2023; Ormerod et al., 2005; Soria et al., 2009). Following such treatments, local rapamycin concentrations are likely to rise to high-enough levels for activation of TRPM8 in sensory nerve endings of the skin, which could potentially contribute to beneficial effects of the drug in certain skin conditions. Indeed, it is well established that activation of TRPM8 in sensory neurons has anti-inflammatory effects and causes relief of pain and itch (Liu et al., 2013; Palkar et al., 2018). Further research is required to elucidate the extent of this contribution and its clinical implications.

In addition to rapamycin, we also tested a comprehensive set of related macrolide immunosuppressants for their effect on TRPM8. In line with earlier work, FK506 also robustly activates TRPM8 (Arcas et al., 2019), albeit with lower potency than rapamycin, whereas the other tested macrolides had only very modest effects. Overall, these findings indicate that the *trans*-2-methoxycyclohexan-1-ol moiety is crucial for activity at TRPM8. Indeed, substitutions at this site (as for instance in everolimus) almost fully abolish TRPM8-mediated responses, whereas activity is at least partially maintained in compounds where this moiety is retained but with altered macrolactam ring (as in FK506 or ascomycin). These findings indicate that the structural

determinants for macrolide activation of TRPM8 differ from the determinants for immunosuppressant activity, which are critically determined by the macrolactam ring (Chen & Zhou, 2020). Notably, we found that everolimus can inhibit activation of TRPM8 by rapamycin but not by menthol, indicating that it likely competes with rapamycin for the same binding site.

Overall, our data are consistent with a macrolide binding site on TRPM8, in the groove between voltage sensor-like domain and the pore domain, distinct from the interaction sites of cooling agents and known TRPM8 agonists menthol and icilin, but partially overlapping with the binding site of AITC. The existence of this binding site is also coherent with the finding of Acras et al. showing that TRPM8 sensitivity to FK506/tacrolimus is not affected by Y745H and N799A mutations which eradicate TRPM8 sensitivity to menthol and icilin, respectively. Notable, this groove is also involved in the binding of the antagonist NDNA in the closely related TRPM5 channel. Alignment of TRPM8 with other TRPM channels indicates that some of the key residues for rapamycin activation (D796 and D802) are conserved amongst other TRPM channels, whereas residue Q861 is unique for TRPM8 and G805 is only found in TRPM8 and TRPM2 (Huffer et al., 2020). Further studies may elucidate whether introduction of these residues may transfer rapamycin sensitivity to other TRPM channels. Moreover, structural alignment indicates that the rapamycin binding site in TRPM8 is in a similar location as the vanilloid binding site in TRPV1, although sequence alignment reveals that the key residues involved in binding are not conserved between these more distally related channels (Cao et al., 2013; Huffer et al., 2020; Kwon et al., 2021) The rapamycin binding site may provide a potential clue for the development of drugs that can selectively target TRPM8 for therapeutic purposes, without the side effects associated with other TRPM8 agonists. We acknowledge the limitations of our docking approach, which did not include the lipid bilayer and its interactions with the channel and ligand (Hughes et al., 2019).

Nevertheless, the integration of docking with experimental validation, such as NMR and detailed calcium imaging and electrophysiology on selected mutants, strengthens the validity of our model. Interestingly, rapamycin also directly activates TRPML1, although information on a possible interaction site on that distally related channel are currently lacking (Zhang et al, 2019). We note that none of the key residues involved in activation of TRPM8 by rapamycin are conserved in TRPML1. Moreover, the order of potency of rapamycin analogs differs substantially between TRPML1 and TRPM8. For instance, TRPML1 is potently activated by temsirolimus, whereas this compound is without agonistic effect at TRPM8 (Zhang et al, 2019).

Finally, our results also serve as a cautionary note for the use of rapamycin in chemical dimerization studies, a common approach in the study of ion channels (Suh et al., 2006; Varnai et al., 2006). To exclude a contribution of TRPM8 in such experiments, the use of rapalogs such as everolimus represents a likely safer alternative.

In conclusion, our study reveals a hitherto undiscovered pharmacological property of rapamycin, identifying it as a direct agonist of the TRPM8 ion channel. These findings provide new insights into ligand activation of TRPM8, and may have potential therapeutic implications in the topical use of rapamycin for the treatment of skin diseases.

METHODS

Cell culture and isolation of sensory neurons

Naive HEK293T cells and HEK293T cells stably overexpressing the human TRPM8 (HEK-M8 cells) were cultured at 37°C in DMEM medium supplemented with 10% fetal bovine serum, , 50 U/ml penicillin, 50 µg/ml streptomycin, 10 mM Glutamax, Non-Essential-Amino-Acids (all from Invitrogen/Thermo Fisher). G418 (500 µg/ml) was added to the medium of HEK-M8 cells.

Experiments using mice were approved by the KU Leuven Ethical Committee Laboratory Animals under project number P006/2014. All experimental procedures and animal husbandry were conducted following the European Parliament and the Council Directive (2010/63/EU) and national legislation. Sensory neurons of from the dorsal root and trigeminal ganglia (DRGs and TGs) were isolated from 8-16-week old wild type (*Trpm8*$^{+/+}$) and TRPM8-deficient (*Trpm8*$^{-/-}$) C57BL6 mice, as described before (Vandewauw et al., 2018). Briefly, mice were euthanized by CO_2, DRGs or TGs were isolated and digested with 1 mg/ml collagenase and 2.5 mg/ml dispase dissolved in 'basal medium' (Neurobasal A medium supplemented with 10% FCS) (all from Gibco/Thermo Fisher) at 37°C for ca. 45–60 min. Digested ganglia were gently washed once in 'basal medium' and twice in 'complete medium' (Neurobasal A medium supplemented with 2% B27 [Invitrogen/Thermo Fisher], 2 ng/ml GDNF [Invitrogen/Thermo Fisher] and 10 ng/ml NT4 [PeproTech, London, UK]) and mechanically dissociated by mixing with syringes fitted with increasing needle gauges. The suspension of sensory neurons was seeded on poly-L-ornithine/laminin-coated glass bottom chambers (Fluorodish, World Precision Instruments, Sarasota, FL USA) and maintained at 37°C for 24 to 36 hrs before experiments.

Microfluorimetric intracellular Ca^{2+} imaging

Fluorescent measurement of the cytoplasmic Ca^{2+} concentration in HEK cells and in individual sensory neurons were performed using the fluorescent Ca^{2+}-sensitive dye Fura-2 AM in various configurations, as reported earlier (Kelemen et al., 2021; Vandewauw et al., 2018).

To measure cytoplasmic Ca^{2+} concentration in individual neurons or HEK-M8 cells, a fluorescence microscope-based calcium imaging system was used. Cells were seeded in glass bottom chambers and next day, they were loaded with 2 µM Fura-2-AM (Invitrogen/Thermo Fisher Scientific) dissolved in normal Ca^{2+}-buffer (150 mM NaCl, 5 mM KCl, 1 mM $MgCl_2x6H_2O$, 2 mM $CaCl_2x2H_2O$, 10 mM glucose xH_2O, 10 mM HEPES, pH 7.4). Fura-2 signals were continuously captured (1 frame/s) using either a CellM (Olympus, Tokyo, Japan) or an Eclipse Ti (Nikon, Tokyo, Japan) fluorescence microscopy system. The cytoplasmic Ca^{2+} concentration was assessed by the ratio of fluorescence measured at λ_{EX1}: 340 nm, λ_{EX2}: 380 nm and λ_{EM}: 520 nm (F_{340}/F_{380}). During the measurements, cells were continuously perfused with buffer and different compounds were applied via rapid perfusion. Experiments were performed at room temperature.

To generate dose response curves and investigate rapalogs and other macrolides, we used a fluorescent microplate reader and monitored a population of HEK-M8 cells in each well. HEK-M8 cells were seeded in Poly-L-Lysine HBr coated 96-well black wall/clear-bottom plates (Greiner Bio-One, Frickenhausen, Germany) at a density of 100,000 cells per well in normal cell culture medium and incubated overnight. Next day, cells were loaded with 2 µM Fura-2-AM at 37°C for 30 min, and washed three times with Ca^{2+}-buffer. Then, changes in cytoplasmic Ca^{2+} concentration (indicated by the ratio of fluorescence measured at λ_{EX1}: 340 nm, λ_{EX2}: 380 nm, λ_{EM}: 510 nm (F_{340}/F_{380})) were measured using either a FlexStation 3 fluorescent microplate reader (Molecular Devices, Sunnyvale, CA, USA) or an FDSS/µCell analysis system (Hamamatsu Kinetic Plate Imager

C13299). In some experiments. fluorescence signals were normalized to baseline values (F_o), and results were expressed as $\Delta F/F_o$ to reflect the relative calcium dynamics. During the measurements, the tested compounds were applied in various concentrations using the built-in pipetting robot of the equipment. In each well, only one given concentration of the agents tested was applied. These measurements were carried out at ambient temperature or at 37 ^oC.

Patch clamp electrophysiology

HEK-M8 cells were seeded on poly-L-lysin coated glass coverslips and transmembrane currents were recorded in the whole-cell or inside-out configurations of the patch-clamp technique using a HEKA EPC-10 amplifier and Patchmaster software (HEKA Elektronik, Lambrecht/Pfalz, Germany). Data were sampled at 5-20 kHz and digitally filtered off-line at 1-5 kHz. Pipettes with final resistances of 2–5 MΩ were fabricated and used to establish a giga-seal access to the membrane. Unless mentioned otherwise, the holding potential was 0 mV and the following voltage step protocol was applied at 0.5 Hz: -80 mV for 200 ms, +120 mV for 200 ms, and -80 mV for 200 ms. In the whole-cell mode, between 70 and 90% of the series resistance was compensated. Whole-cell recordings were performed using an intracellular solution in the patch pipette containing (in mM) 150 NaCl, 5 MgCl2, 5 EGTA and 10 HEPES, pH 7.4 with NaOH. The extracellular solution contained (in mM) 150 NaCl, 1 MgCl2 and 10 HEPES, pH 7.4 with NaOH. In inside-out recordings, the extracellular solution was used as pipette solution, and ligands were applied via the intracellular bath solution.

In patch-clamp experiments where intracellular Ca^{2+} was manipulated through flash photolysis of caged Ca^{2+}, the pipette solution contained (in mM): 120 NaCl, 2 Fura-2FF and 20 HEPES, pH 7.4 with NaOH. This solution was further supplemented with 2 mM of the photolysable calcium chelator DM-nitrophen and 1.5 mM $CaCl_2$. Intracellular Ca^{2+} was monitored using a mono-

chromator based system consisting of a Polychrome IV monochromator and photodiode detector (TILLPhotonics, Gräfelfing, Germany), controlled by Patchmaster software . Fluorescence was measured during excitation at alternating wavelengths (350 and 380 nm), corrected by subtraction of the back-ground fluorescence before establishing the whole-cell configuration, and represented as F_{350}/F_{380}. Rapid photolytic release of Ca^{2+} was achieved by subjecting the cell to brief (~1 ms) UV flashes applied from a JML-C2 flash lamp system (Rapp OptoElectronic GmbH, Hamburg, Germany), leading to step-wise, spatially uniform increases in intracellular Ca^{2+} (Mahieu et al., 2010).

Saturation Transfer Triple-Difference (STTD) NMR spectroscopy

^{1}H STD NMR experiments were performed on a Bruker Avance Neo 700 MHz spectrometer equipped with a 5-mm z-gradient Prodigy TCI cryoprobe. The temperature was maintained at 298 K. The ^{1}H reference experiments were run with 256 number of scans, a 1.2 s relaxation delay, and a watergate sequence was utilized for water suppression. These spectra were used to assess sample stability and to scale STD effects (Figure S5). A train of 50-ms Eburp1 (with B_1 field strength of 75 Hz) was employed for selective irradiation of protein ^{1}H resonances in total of 3 s. The saturation of aliphatic and aromatic proton regions of TRPM8 was carried out in separate experiments by setting the irradiation (on-resonance) frequencies of -1.8 ppm and 8.8 ppm, respectively, at least 2 ppm away from the resonances of rapamycin to avoid any partial saturation of rapamycin ^{1}H resonances. Reference spectra were recorded by setting the irradiation frequency off-resonance at -40 ppm. A spin-lock filter of 20 ms was applied to reduce the broad signals of the receptor and cell components in the resulting STD spectra. For each STD spectrum (the two on-resonance and one off-resonance) 640 number of scans was acquired in an interleaved fashion to average out any sample and/or spectrometer instability during the

measurement, resulting in a total experiment time of 3 hours. All spectra were processed with Topspin version 4.0.5.

NMR samples: $25x10^6$ HEK293T or HEK-M8 cells/sample were used. Cells were counted by a NovoCyte flow cytometer (Agilent Technologies), and the number of the functional TRPM8 channels were estimated as ca. 5000 channels/cell based on average whole cell currents and single channels conductance available in the literature. 5 µl of rapamycin was added from a 22 mM stock solution resulting in a final concentration of 0.2 mM in D_2O PBS solution, providing ca. $4.8x10^7$-fold excess of ligand to TRPM8 ion-channels for the STD NMR measurements. The final volume of each sample was 550 µl. NMR data was recorded in three replicates, a total of 12 individual samples were used to compute three independent STTD spectra (Figure S6).

Synthesis of trans-2-Methoxycyclohexan-1-ol

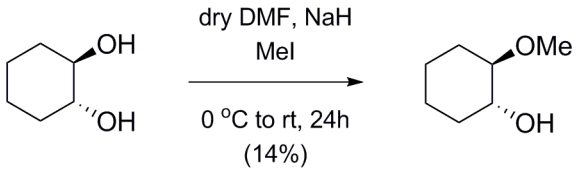

Trans-2-Methoxycyclohexan-1-ol was synthetized based on the method of Winstein and Henderson (Winstein & Henderson, 1943). To the solution of ***trans*-1,2-cyclohexanediol** (500 mg, 4.304 mmol) in dry DMF (19 mL) NaH (413 mg, 10.329 mmol, 60 m/m%, 1.2 equiv./OH) was added at 0°C. After 30 min stirring at that temperature 308 µl MeI (4.949 mmol, 1.15 equiv.) was added to the mixture and stirred for 24 h. When the TLC analysis (9:1 CH_2Cl_2/MeOH) showed complete consumption of the starting material, the reaction mixture was quenched by the addition of MeOH (2.5 mL). The solution was concentrated under reduced pressure and the residue was dissolved in CH_2Cl_2 (150 mL) washed with H_2O, dried on $MgSO_4$ and concentrated. The crude

product was purified by column chromatography on silica gel (9:1 CH_2Cl_2/MeOH) to give ***trans*-2-methoxycyclohexan-1-ol** (80 mg, 14%) as a colorless syrup. $[\alpha]_D$ −6.54 (*c* 0.26, $CHCl_3$); R_f 0.47 (95:5 CH_2Cl_2/MeOH); ^{1}H NMR (400 MHz, $CDCl_3$) δ = 3.44-3.38 (m, 4H, OC*H*$_3$, H-1), 3.10 (s, 1H, H-1-O*H*), 2.94 (ddd, *J* = 10.6 Hz, *J* = 8.7 Hz, *J* = 4.4 Hz, 1H, H-2), 2.14-1.03 (m, 8H, 4 x C*H*$_2$), ppm; ^{13}C NMR (100 MHz, $CDCl_3$) δ = 85.0 (1C, C-2), 73.6 (1C, C-1), 56.3 (1C, O*C*H$_3$), 32.2, 28.4, 24.1, 24.0 (4C, 4x *C*H$_2$) ppm; MS (UHR ESI-QTOF): *m/z* calcd for $C_7H_{14}NaO_2$, $[M+Na]^+$ 153.0886; found: 153.0885.

Molecular docking

Initial docking simulations were performed using the cryo-EM structure of the full-length collared flycatcher (*Ficedula albicollis*) TRPM8 (pdb code: 6NR2, 83% sequence identity to human TRPM8) (Yin et al., 2019) high-resolution structures of rapamycin (pdb codes: 5FLC, 5GPG) retrieved from the RCSB Protein Data Bank.

Pilot dockings were performed using the Autodock 4.2 software in a 98.0 Å x 98.0 Å x 58.0 Å grid volume, large enough to cover the transmembrane domains of all four subunits of TRPM8 accessible from the extracellular side. The spacing of grid points was set to 1.0 Å and the whole target protein structure and the macrocyclic backbone of the ligand were kept rigid during dockings. 5000 dockings were performed with the above settings and the resultant rapamycin-TRPM8 complexes were clustered and ranked according to the corresponding binding free energies.

Internal flexibility of the rapamycin molecule was assessed through performing simulated annealing using the Gromacs 5.1.4 software package, the CHARMM36 force field and the GB/SA continuum solvent model. The simulated annealing protocol consisted of 2-ps gradual heating from 50 K to 1050 K, 5-ps equilibration at 1050 K and 5-ps exponential cooling back to 50 K. This

protocol was repeated 1000 times for both crystallographic models of rapamycin. The coordinates of the system were stored after each simulated annealing cycle, resulting in a 1000-member ensemble of low-energy structures for both initial rapamycin models. Representative conformations of rapamycin were identified by clustering of the 1000-membered pools, having the macrocycle backbone atoms compared with 1.0 Å RMSD cut-off. Middle structures of the ten most populated clusters, accounting for more than 90% of the total conformational ensemble generated by simulated annealing, were used for further docking studies. To refine initial docking results and to identify plausible binding sites, the above selected rapamycin structures were docked again to the protein target, following the same protocol as above, except for the grid spacing which was set to 0.375 Å in the second pass. The resultant rapamycin-TRPM8 complexes were, again, clustered and ranked according to the corresponding binding free energies. Selected binding poses were subjected to further refinement.

The three most populated and plausible binding poses were further refined by a third pass of docking, where amino acid side chains of TRPM8, identified in the previous pass to be in close contact with rapamycin (< 4 Å), were kept flexible. Grid volumes were reduced to these putative binding sites including all flexible amino acid side chains (21.0-26.2 Å x 26.2-31.5 Å x 24.8-29.2 Å). The spacing of grid points was maintained at 0.375 Å. Putative binding modes of rapamycin and TRPM8 were selected from the resultant low energy complexes on the basis of adherence to STTD-NMR data and the number of direct intermolecular contacts.

The initial dockings were further refined upon the publication of Cryo-EM structures of the mouse TRPM8 variant (Yin et al., 2022). The hTRPM8 protein sequence Q7Z2W7 was downloaded from the Universal Protein Resource (UniProt) and template Cryo-EM structures of mTRPM8 cold receptor in apo state C1 (PDB ID: 8E4N) and apo state C0 (PDB ID: 8E4P) were downloaded from

the Protein Data Bank. The homology modelling was performed with the standard homology modelling protocol implemented in Yasara (https://www.yasara.org). Homology model based on these cryo-EM structures were performed using Swiss model as well with GMQE=0.71 and sequence identity=93.74%. All the structures were repaired using the FoldX plugin in YASARA, where RepairPDB identifies those residues which have bad torsion angles, or VanderWaals' clashes, or total energy, and repairs them. Visualization of the molecules was also done with Yasara. Figures were drawn with the open source Pymol (The PyMOL Molecular Graphics System, Version 2.5.2 Schrödinger, LLC; available at https://www.pymol.org). The global docking procedure was accomplished with Autodock VINA algorithms, implemented in Yasara, in which a total of 900 docking runs were set and clustered around the putative binding sites. The grid volumes and parameters were similar to those used for the third pass of docking, described above. The Yasara pH command was set to 7.0, to ensure that molecules preserved their pH dependency of bond orders and protonation patterns. The best binding energy complex in each cluster was stored, analyzed, and used to select the best orientation of the interacting partners. Using a similar docking strategy, we reproduced binding of menthol into the reported menthol binding site based on the cryo-EM structure of TRPM8 in complex with the menthol-analog WS-12 (Yin et al., 2019).

Generation of hTRPM8 mutants

Based on the results of the *in silico* studies, mutations were introduced at strategic sites within the putative ligand-binding domains. Single amino acids in the full length human TRPM8 sequence were mutated using the standard PCR overlap extension technique (Voets et al., 2007), and the nucleotide sequences of all mutants were verified by DNA sequencing. Constructs were cloned in the bicistronic pCAGGSM2-IRES-GFP vector, transiently expressed in HEK293 cells using TransIT-

293 transfection reagent (Mirus, Madison, WI), and characterized using whole-cell patch-clamp electrophysiology and single cell calcium microfluorimetry as described above.

Chemicals

Rapamycin, FK506 ascomycin, everolimus, and temsirolimus were purchased from LC Laboratories (Woburn, MA USA***).*** Unless indicated otherwise, all other chemicals were obtained from Sigma-Aldrich.

Data analysis and statistics

Data analysis and statistical tests were performed using Origin software (9.0 or 2023; OriginLab). Data are represented as mean ± SEM from *n* cells. One-way ANOVA with a Tukey post-hoc test was used to compare the effect of multiple mutations on TRPM8 ligand responses. Differences in the response profile of somatosensory neurons between genotypes were analyzed using Fisher's exact test. $P < 0.05$ was considered as statistically significant.

Concentration-response curves were fitted using the Hill equation of the form:

$$Response = \frac{Response_{max}}{1 + \left(\frac{EC_{50}}{[C]}\right)^{n_H}}$$

where the calculated parameters are the maximal calcium or current response ($Response_{max}$), the concentration for half-maximal activation (EC_{50}) and the Hill coefficient (n_H). To quantify ligand-induced changes in the time course of voltage-dependent current relaxation during voltage steps, mono-exponential functions were fitted to the current traces. While currents in the presence of

agonists such as menthol or rapamycin become multiexponential, the monoexponential fits provide a robust quantification of changes in relaxation kinetics.

FIGURES

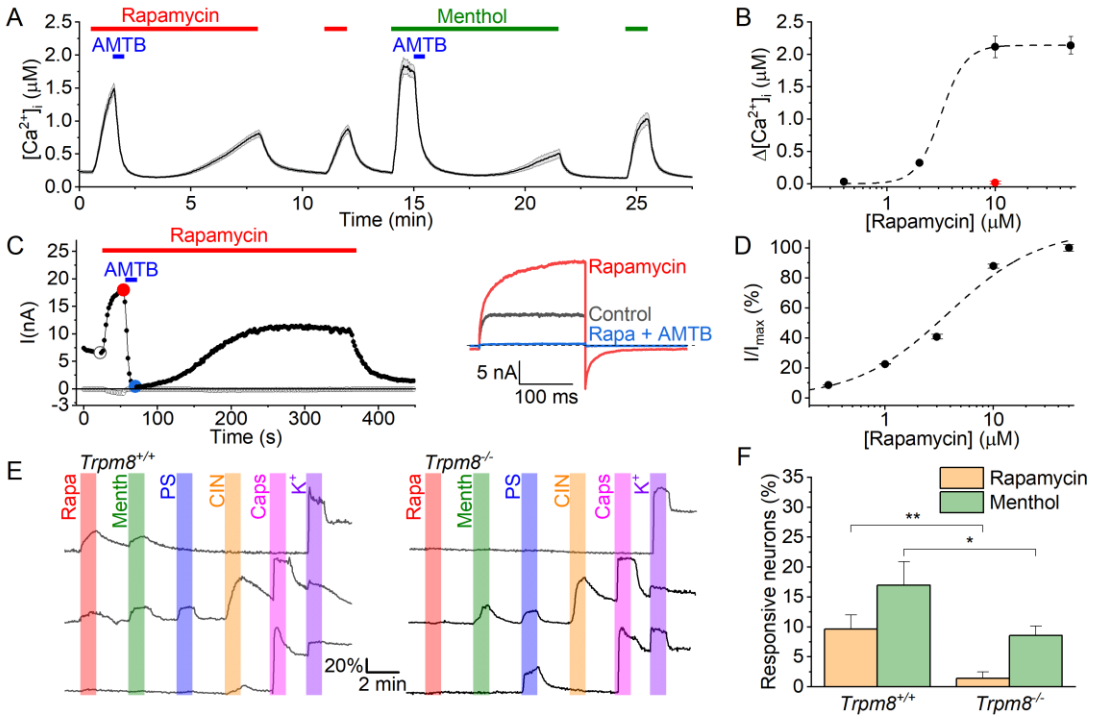

Figure 1: Rapamycin activates TRPM8 in HEK293 cells and sensory neurons.

(A) Time course of the intracellular calcium concentration in HEK293 cells expressing TRPM8, showing robust responses to rapamycin (10 µM) and menthol (50 µM), and inhibition of the responses by AMTB (2 µM). Shown are mean ± SEM, N=63 cells

(B) Concentration dependence of rapamycin-evoked calcium responses. The dashed line respresents the best fit using a Hill equation (EC_{50}=3.1; n_H=3.8). Shown are mean ± SEM, N=52-95 cells/concentration. The red symbol indicates the lack of response to rapamycin (10 µM) in non-transfected HEK293 cells (N=23).

(C) *Left,* time course of whole-cell currents in HEK293 cells expressing TRPM8 evoked by repetitive voltage steps to +120 and -80 mV, showing the activation of outwardly rectifying currents by rapamycin (10 µM) and inhibition by AMTB (2 µM). *Right,* voltage steps recorded at the indicated time points.

(D) Concentration dependence of rapamycin-evoked whole-cell currents at +120 mV. The dashed line respresents the best fit using a Hill equation (EC_{50}=3.8; n_H=1.0). Shown are mean ± SEM, N=5 cells per concentration

(E) Examples of calcium signals in individual DRG neurons from $Trpm8^{+/+}$ and $Trpm8^{-/-}$ mice in response to rapamycin (Rapa; 10 µM), menthol (Menth; 50 µM), pregnenolone sulphate (PS; 40 µM), cinnamaldehyde (CIN; 10 µM), capsaicin (Caps; 100 nM) or high K^+ (50 mM).

(F) Fraction of sensory neurons from Trpm8$^{+/+}$ and Trpm8$^{-/-}$ mice that responded to rapamycin and menthol.

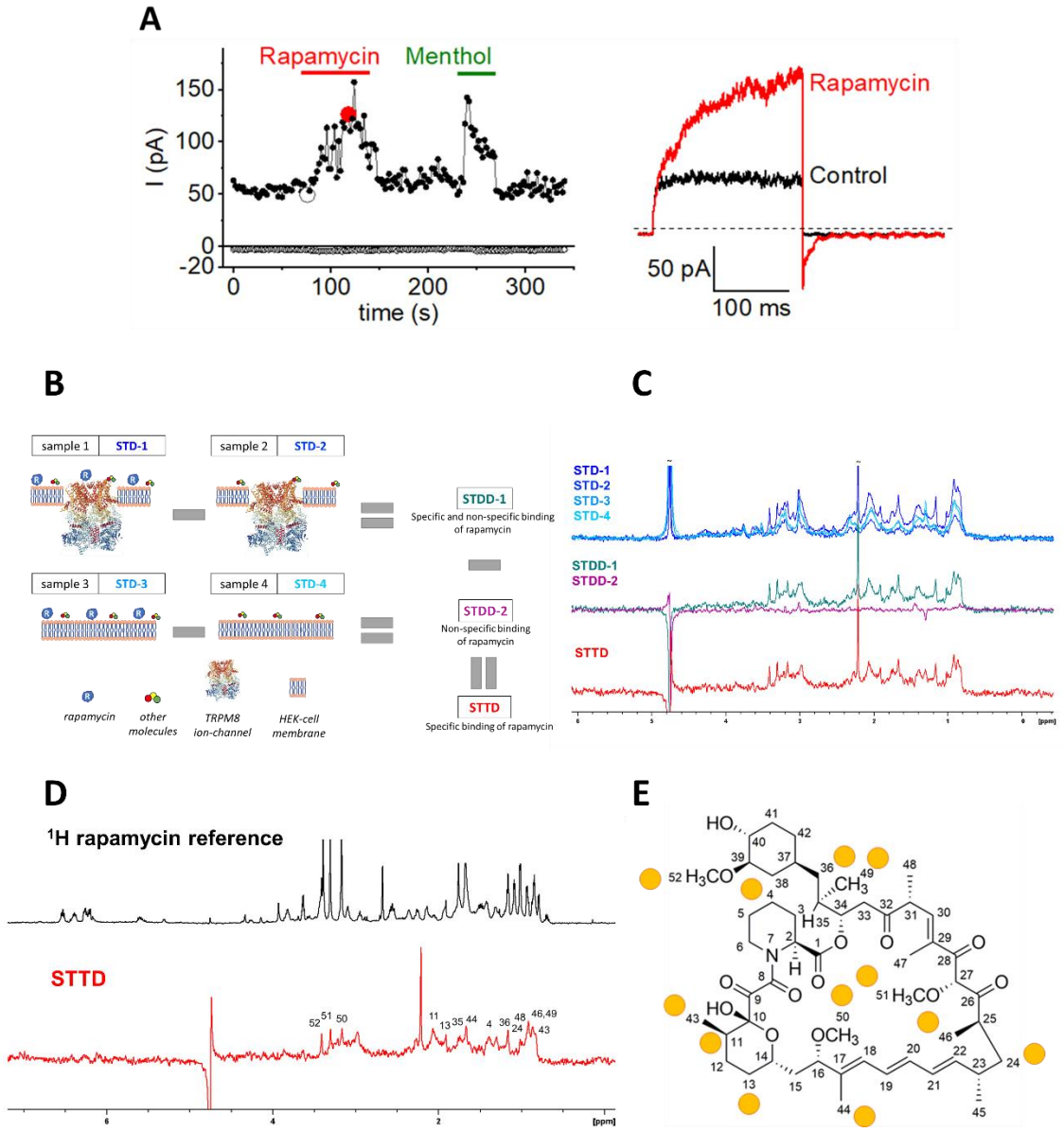

Figure 2: Direct interaction between rapamycin and TRPM8.

(A) *Left,* time course of currents in a cell-free inside-out patch pulled from a HEK293 cell expressing TRPM8 evoked by repetitive voltage steps to +80 and -80 mV, showing the activation of outwardly rectifying currents by rapamycin (10 µM) and menthol (50 µM) applied from the cytosolic side. *Right,* voltage steps recorded at the indicated time points. This example is representative for 5 similar experiments.

(B) Cartoon representing the steps to obtain the direct interaction of rapamycin with TRPM8. Individual STD spectra were recorded on different sample compositions, then non-specific

interactions were filtered out with multiple subtractions resulting in the double difference spectra (STDD-1,2) and the final triple difference spectrum (STTD) shown on the right side.

(C) The four STD spectra (STD-1,2,3,4) are overlayed for comparison. Double difference spectra were computed from the respective STD pairs showing the specific and non-specific binding of rapamycin (STDD-1, green) and the non-specific binding of rapamycin alone (STDD-2, purple). All non-specific interactions were filtered out in the final STTD spectrum (red) computed by subtracting STDD-2 from STDD-1. Here, only one experimental set is shown (dataset B), spectra on the replicates can be found in the supplementary (Figures S5 and S6).

(D) Rapamycin resonances involved in the direct interaction with TRPM8 were assigned by the comparison of the reference ^{1}H NMR spectra of rapamycin (black) with the computed STDD effects (red). The reference spectrum was recorded on a 0.2 mM rapamycin sample in a D_2O buffer solution at 25 °C. The number of scans was 256 and a watergate sequence was used to suppress the residual water signal.

(E) Hydrogen atoms involved in the interaction with TRPM8 are mapped to the structure of rapamycin (yellow circles).

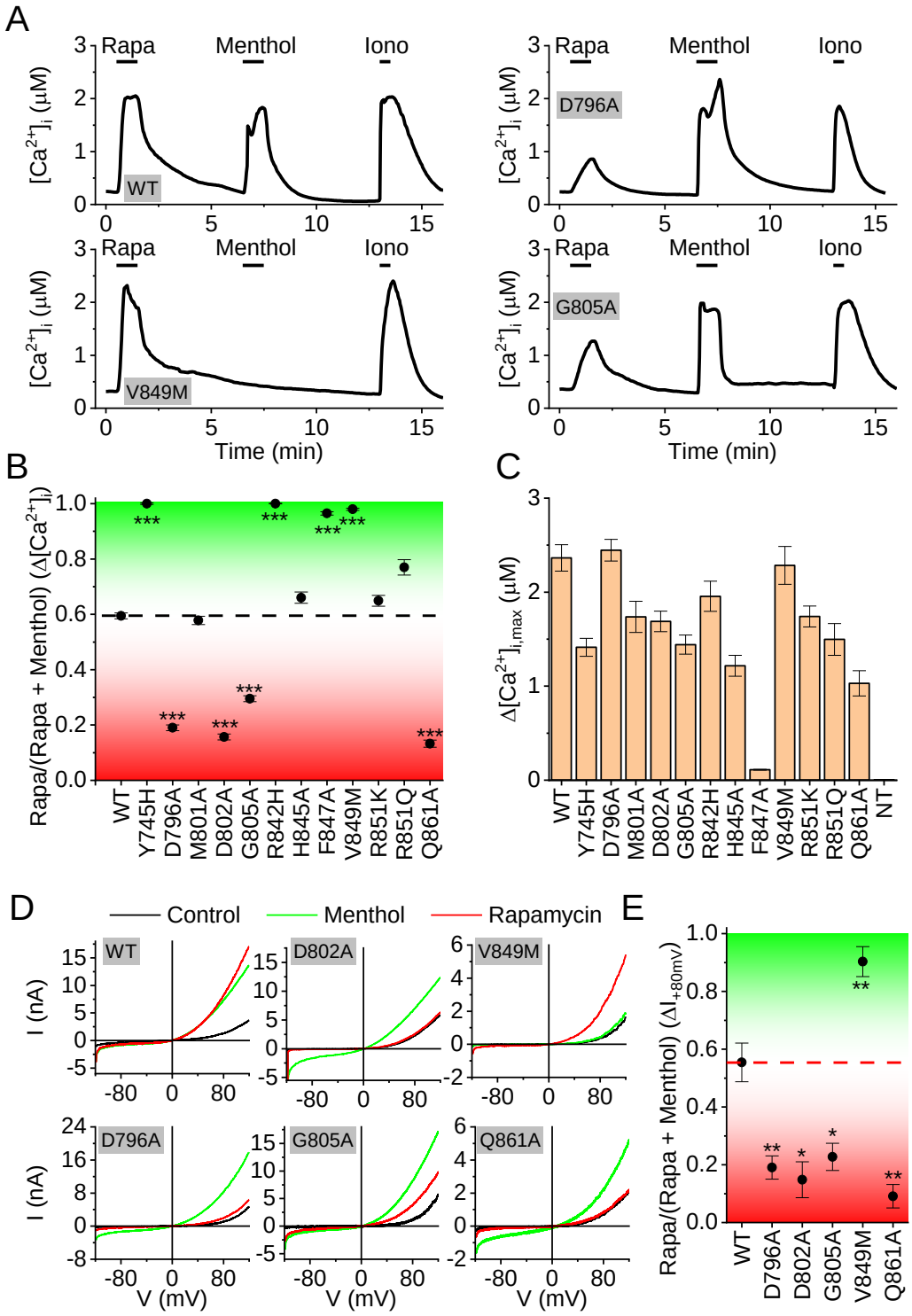

Figure 3: TRPM8 residues involved in the interaction with rapamycin and menthol.

(A) Representative time courses of the intracellular calcium concentration in HEK293 cells expressing wild type TRPM8 or the indicated mutants, when stimulated with rapamycin (10 µM), menthol (50 µM) and the calcium ionophore ionomycin (2 µM).

(B) Quantification of the relative calcium response to rapamycin and menthol for wild type and the indicated TRPM8 mutants. Values indicate the ratio between the calcium response amplitude to rapamycin, divided by the sum of the responses to rapamycin and menthol. The dotted line represents the mean value for wild type TRPM8. Values above this line (in yellow) indicate a relative reduction in the response to menthol, whereas values below the line (cyan) indicate a relative reduction in the response to rapamycin.

(C) Amplitude of the calcium response to the agonist (menthol or rapamycin) that gave the largest response for wild type and the indicated TRPM8 mutants. Data in B and C represent mean ± SEM, N=34-156/group.

(D) Whole-cell current-voltage relations for the currents in control, and in the presence of rapamycin (10 µM) or menthol (50 µM) in HEK293 cells expressing wild type TRPM8 or the indicated mutants.
*, **, *** indicate $p<0.05$, $p<0.01$ and $p<0.001$ compared to WT.

(E) Quantification of the relative current response to rapamycin and menthol for wild type and the indicated TRPM8 mutants. Values indicate the ratio between the current amplitude increase at +80 mV to rapamycin, divided by the sum of the responses to rapamycin and menthol. The dotted line represents the mean value for wild type TRPM8. Values above this line (in yellow) indicate a relative reduction in the response to menthol, whereas values below the line (cyan) indicate a relative reduction in the response to rapamycin. Data in represent mean ± SEM; N=5-8 per mutant.

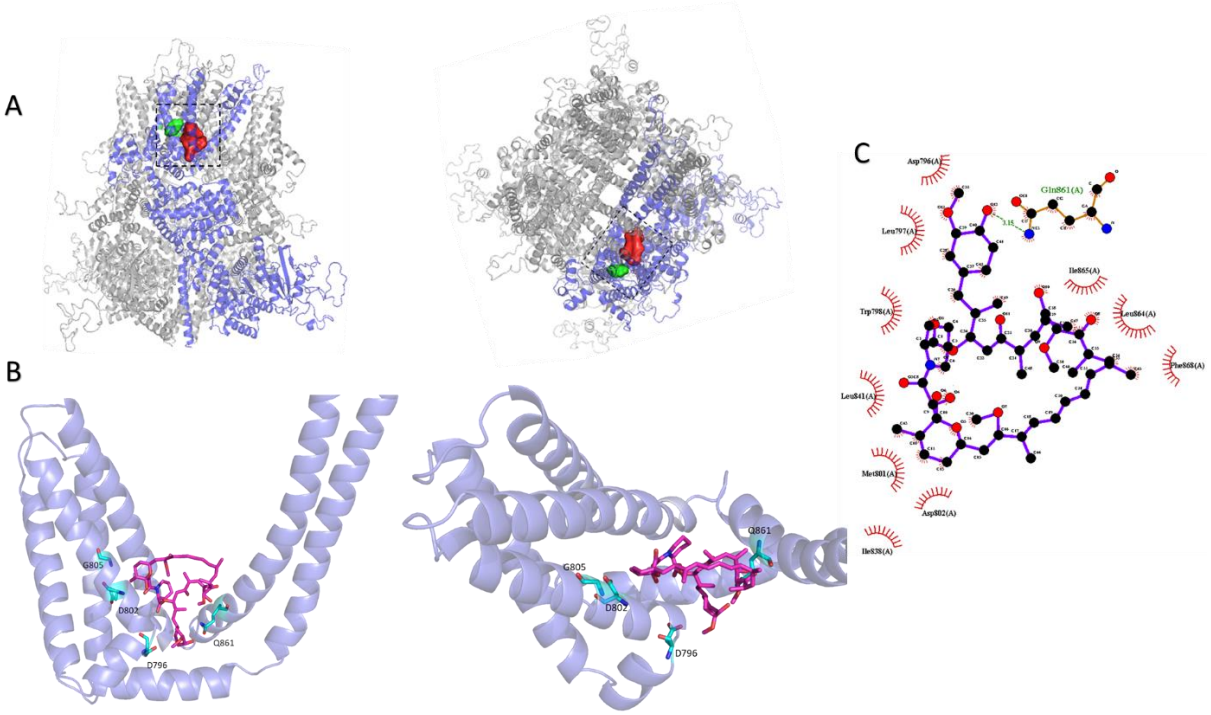

Figure 4: Structural model showing the distinct interaction sites for menthol and rapamycin .

(A) Side view (*left*) and top view (*right*) of TRPM8, showing the known interaction site for menthol (green) and the proposed rapamycin interaction site (red) based on our present molecular docking and mutagenesis studies.

(B) Closer view of rapamycin docked onto the TRPM8 structure. Amino acid residues that, when mutated, influence rapamycin responses are indicated in green.

(C) 2D projection of interactions between rapamycin and TRPM8 created using Ligplot[+].

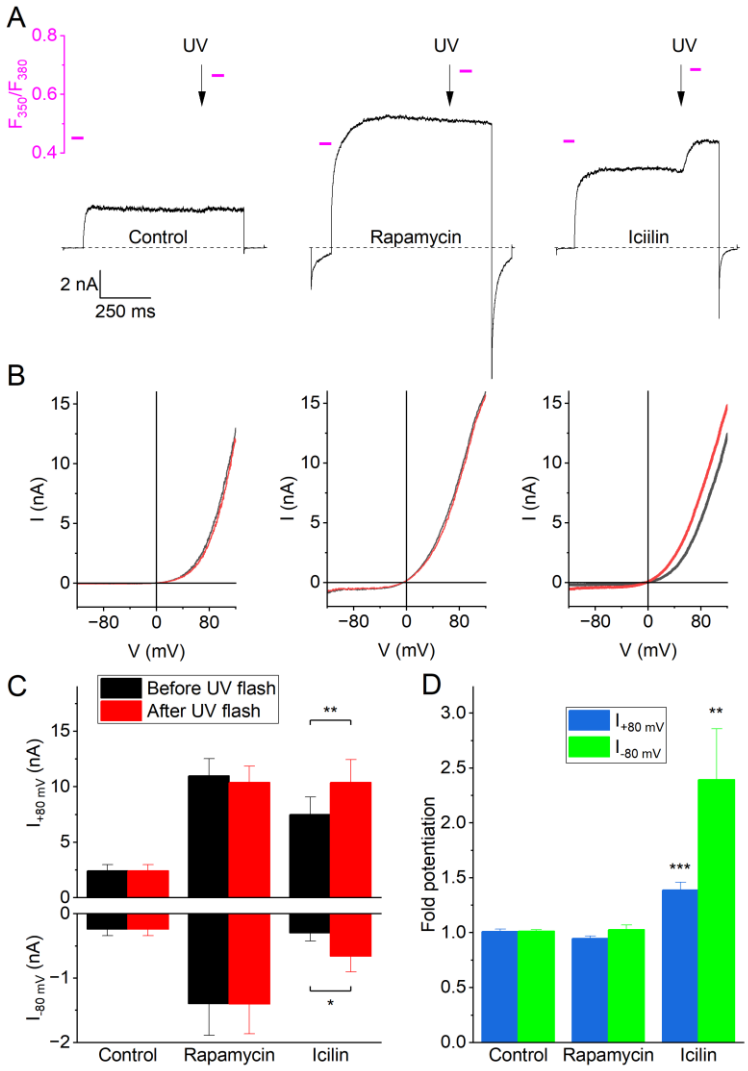

Figure 5: Activation of TRPM8 by rapamycin is independent of intracellular calcium.

(A) Whole-cell currents during 800-ms voltage steps from -80 to +80 mV under control conditions and in the presence of rapamycin (10 µM) or icilin (10 µM). At the time points indicated by the arrows, a 1-ms UV falsh was applied, leading to a rapid increase in intracellular calcium. Magenta lines and scale bar indicate Fura-FF fluoresence ratios at the indicated time points.

(B) Whole-cell current-voltage relations measured during voltage ramps 2 s before and 1 second after the UV flashes shown in panel A.

(C) Current amplitudes at +80 and -80 mV before and after UV uncaging of calcium, under control conditions and in the presence of rapamycin or icilin.

(D) Quantification of the relative potentiation of inward and outward currents following UV uncaging of calcium. Data in C and D represent the mean ± SEM from 5 experiments.
*,**, ***: $p<0.05$ in a paired t-test comparing currents before and after UV flash.

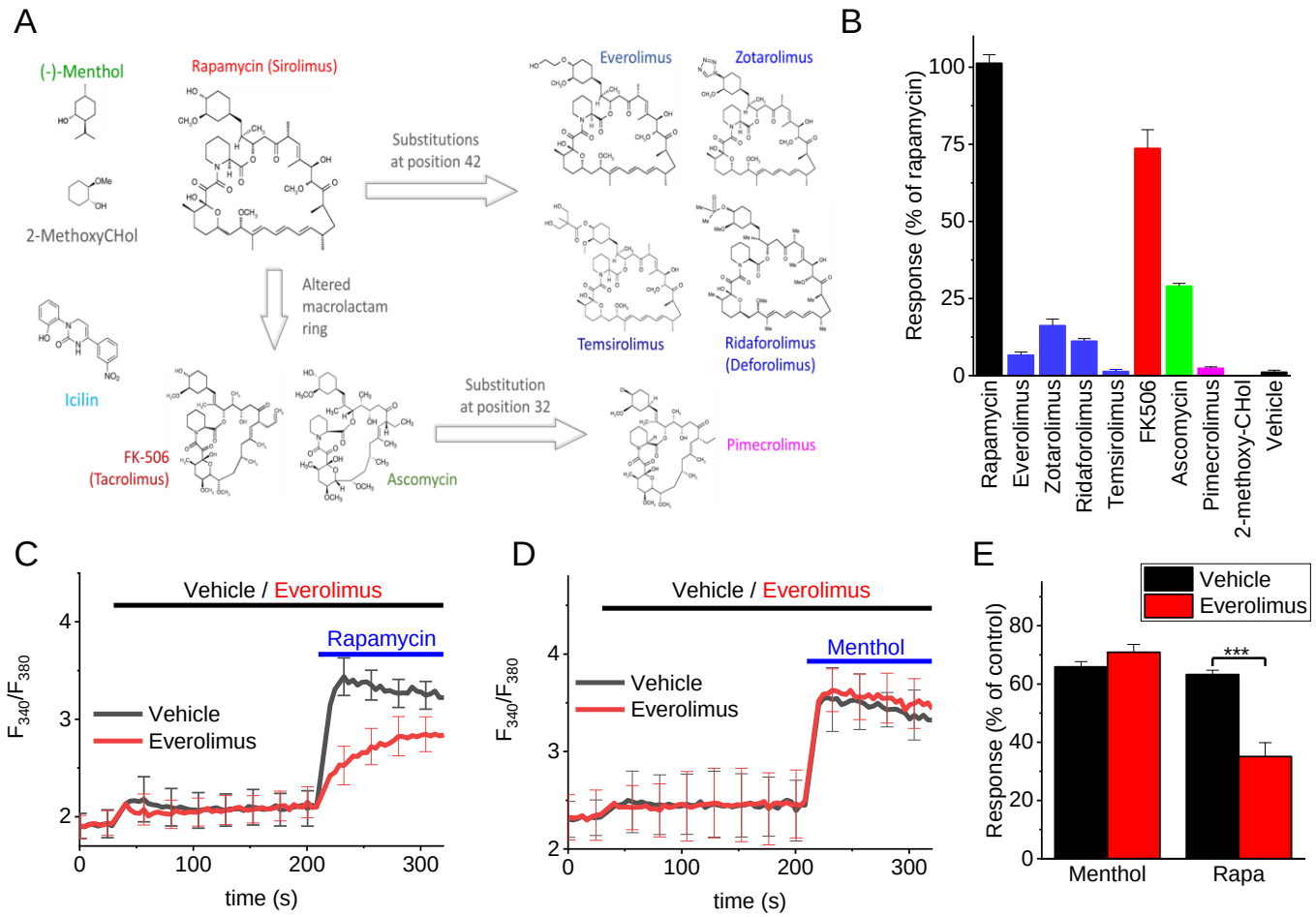

Figure 6: Effect of rapamycin and macrolid analogs on TRPM8 .

(A) Overview of the macrolids tested in this study.
(B) Relative calcium response to rapamycin and the indicated analogs tested at 10 µM. N=6 in each group.
(C) Fura2-based calcium response to rapamycin (10 µM) in the presence of everolimus (10 µM) or vehicle. N=6 in each group.
(D) Fura2-based calcium response to menthol (50 µM) in the presence of everolimus (10 µM) or vehicle. N=6 in each group.
(E) Summary of the responses to menthol (50 µM) and rapamycin (10 µM) in the absence or presence of everolimus (10 µM). Responses were normalized to the response to a saturating concentration of menthol (300 µM). N=6 in each group.
***: $p<0.001$.

SUPPLEMENTARY FIGURES

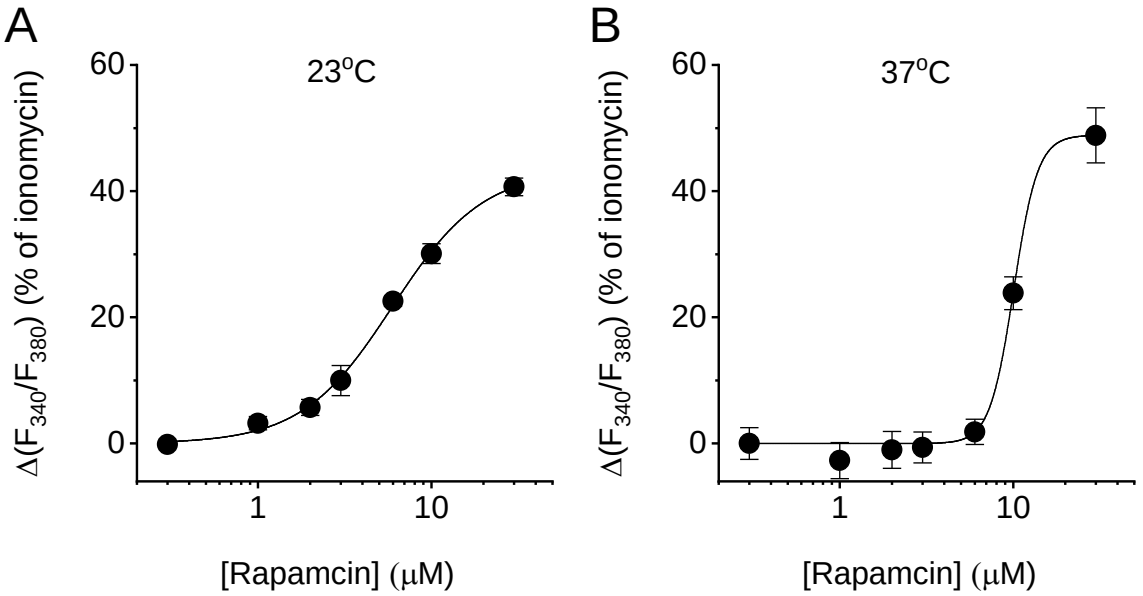

Figure S1: Rapamycin activates hTRPM8 in a concentration-dependent manner.

(A-B) Concentration dependence of rapamycin-evoked calcium responses measured by a microplate reader at room temperature (23 °C) (A) and 37°C (B). Shown are mean ± SEM; N=5 wells for each concentration. The lines represent the best fit using a Hill equation, yielding EC_{50} values of 6.0 ± 0.3 μM and 10.1 ± 0.2 μM, and Hill coefficients of 1.9 and 4.8, at 23°C and 37°C respectively.

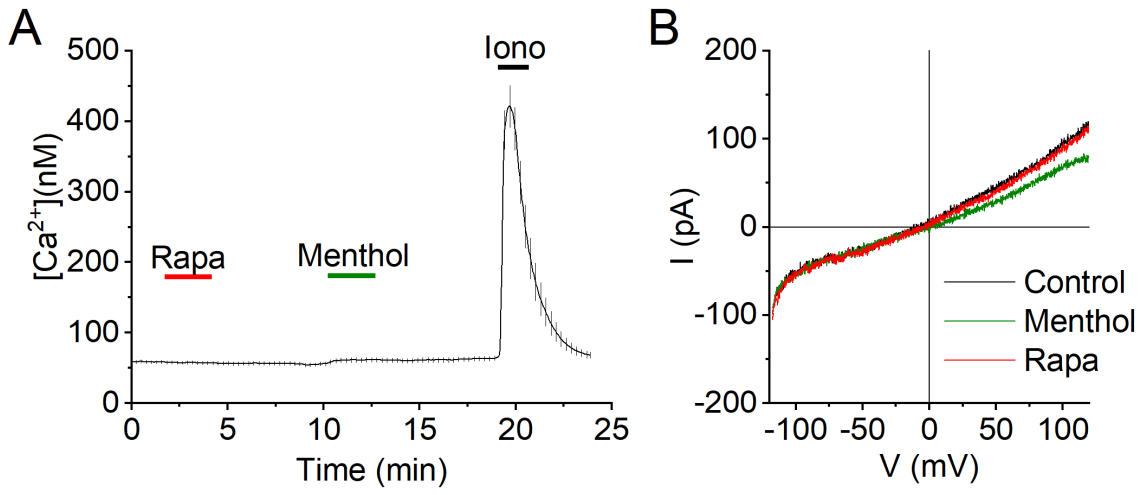

Figure S2: Rapamycin does evoke calcium signals in naïve HEK293 cells.

(A) Time course of the intracellular calcium concentration in non-transfected HEK293 cells, when stimulated with rapamycin (10 µM), menthol (50 µM) and the positive control stimulus ionomycin (2 µM). Shown are mean ± SEM, N=23 cells.

(B) Whole-cell current-voltage relations obtained in non-transfected HEK293 cells, using the same approach as used for wild type and mutant TRPM8 in Figure 3D. In N=5 similar experiments, changes in current amplitude upon addition of menthol or rapamycin never exceeded 50 pA at -100 and +100 mV.

mTRPA1

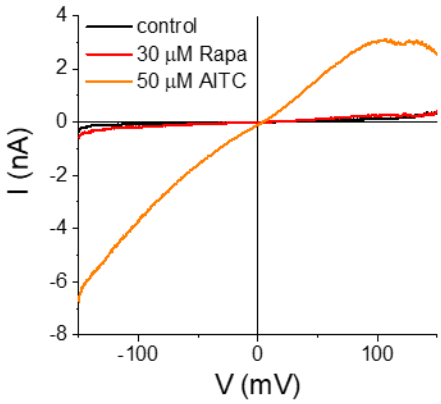

mTRP3α2

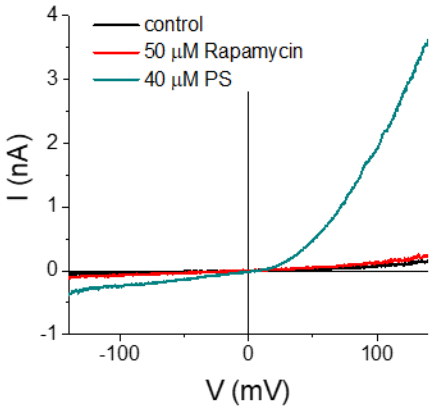

mTRPV1

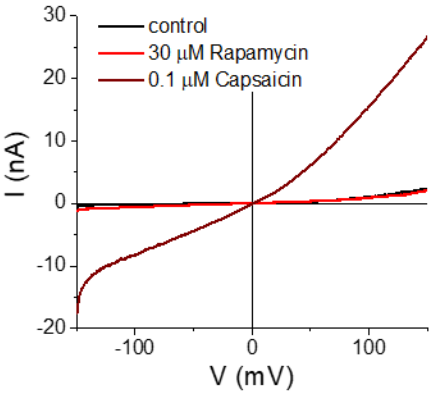

Figure S3: Rapamycin does not activate TRPA1, TRPM3 or TRPV1.

(A-C) Representative whole-cell current-voltage relations in CHO-cells expressing mouse TRPA1 (A), HEK293 cells expressing mouse TRPM3 (B) or HEK293 cells expressing human TRPV1 (C) upon stimulation with rapamycin (30 µM) or the respective agonists Allyl isothiocyanate (AITC), pregnenolone sulphate (PS; 40 µM) and capsaicin (Caps; 100 nM). Current responses to rapamycin where <5% of the response to the respective channel agonists in n=5 cells.

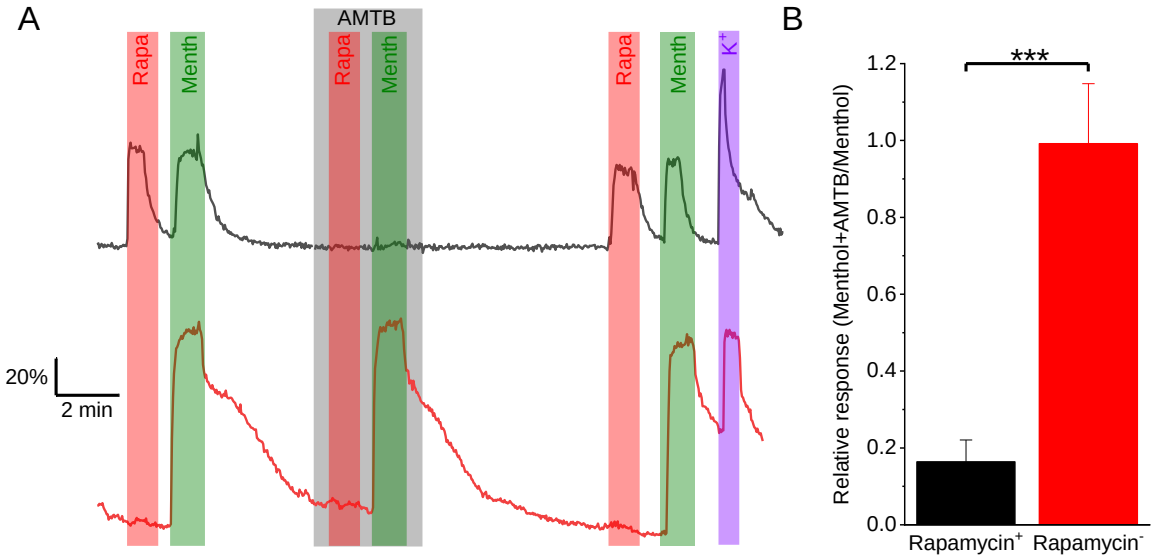

Figure S4: Rapamycin allows distinghuising between TRPM8-mediated and TRPM8-independent menthol responding sensory neurons.

(A) Representative examples of Fura2-based calcium signals in two sensory neurons that were stimulated three times at the indicated times with rapamycin (10 µM) or menthol (50 µM). During the second application, the TRPM8 antagonist AMTB was present at a concentration of 2µM.

(B) Average ratio between the response to menthol in the presence and absence of AMTB (second response/first response) in neurons that did or did not respond to rapamycin.

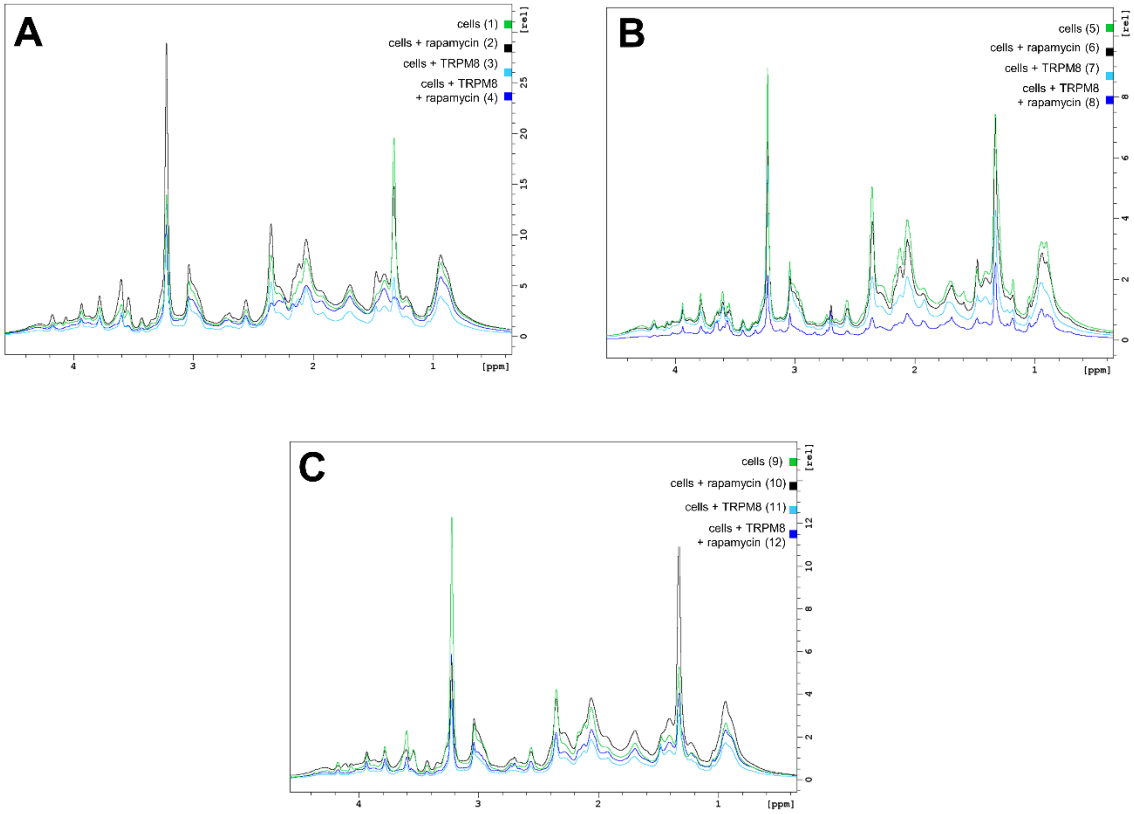

Figure S5. The variability of peak heights in ^{1}H NMR experiments and the normalization procedure.

Reference ^{1}H experiments are shown on three individual sets of samples from which later three parallel STTD spectra were computed by the linear combinations of STD experiments. Conditions and sample numbering are shown in the right corner of the plots. The size of the spectra varied significantly despite the strict production protocol due to the complexity of the samples. Therefore, the scaling of the follow-up STD experiments was performed prior to the linear combinations based on the peak integral sums from the 0-4 ppm region of ^{1}H experiments. The corresponding STD spectra were scaled to an external spectrum recorded on a cell sample with an overexpressed ion channel and rapamycin. The following factors were used for multiplication: Dataset A: (1): 0.29, (2): 0.24, (3): 0.48, (4): 0.40. Dataset B: (5): 0.70, (6): 0.82, (7): 1.05, (8): 4.92. Dataset C: (9): 0.34, (10): 0.28, (11): 0.60, (12): 0.46.

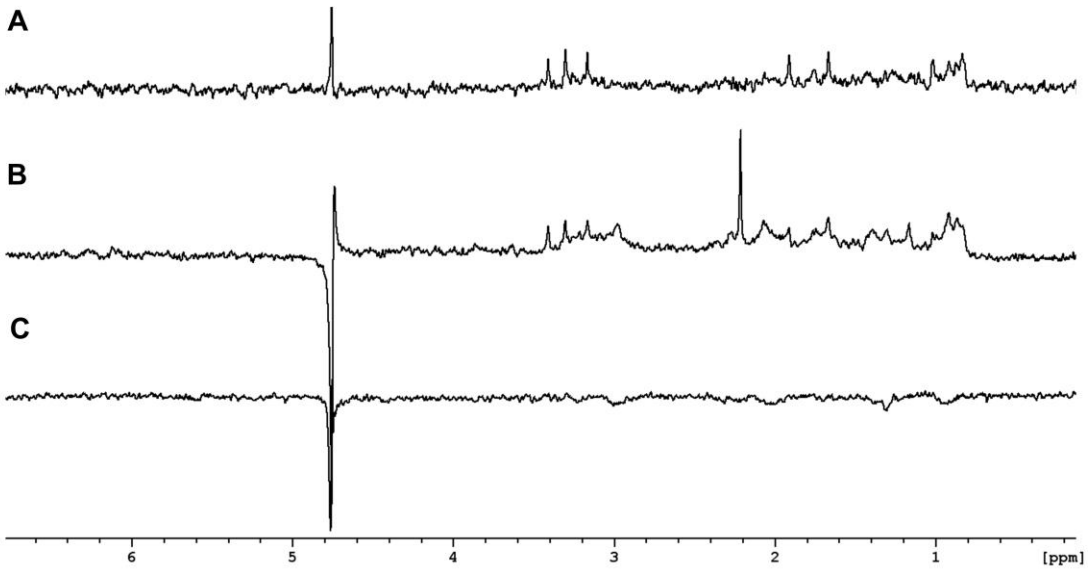

Figure S6. Replicates of STTD measurements.

(A) An STTD spectrum obtained by the linear combinations of scaled STD spectra [(4-3) - (2-1)]. A direct interaction between rapamycin and the ion channel is confirmed and interaction sites of rapamycin were revealed upon peak assignments (presented in Figure 2).

(B) An STTD spectrum obtained by the linear combinations of scaled STD spectra [(8-7) - (6-5)]. A direct interaction between rapamycin and the ion channel is confirmed and the same interaction sites of rapamycin were revealed upon peak assignments.

(C) An STTD spectrum obtained by the linear combinations of scaled STD spectra [(12-11) - (10-9)]. Here, there is no reliable STD effect confirming the direct interaction between TRPM8 and rapamycin. Increased cell sedimentation was observed in sample 12 after measurements, an unconotrolled process that might have reduced the detected STD effects. Consequently the extent of non-specific binding outweighed specific binding resulting in zero or „negative" effects in the STTD spectrum.

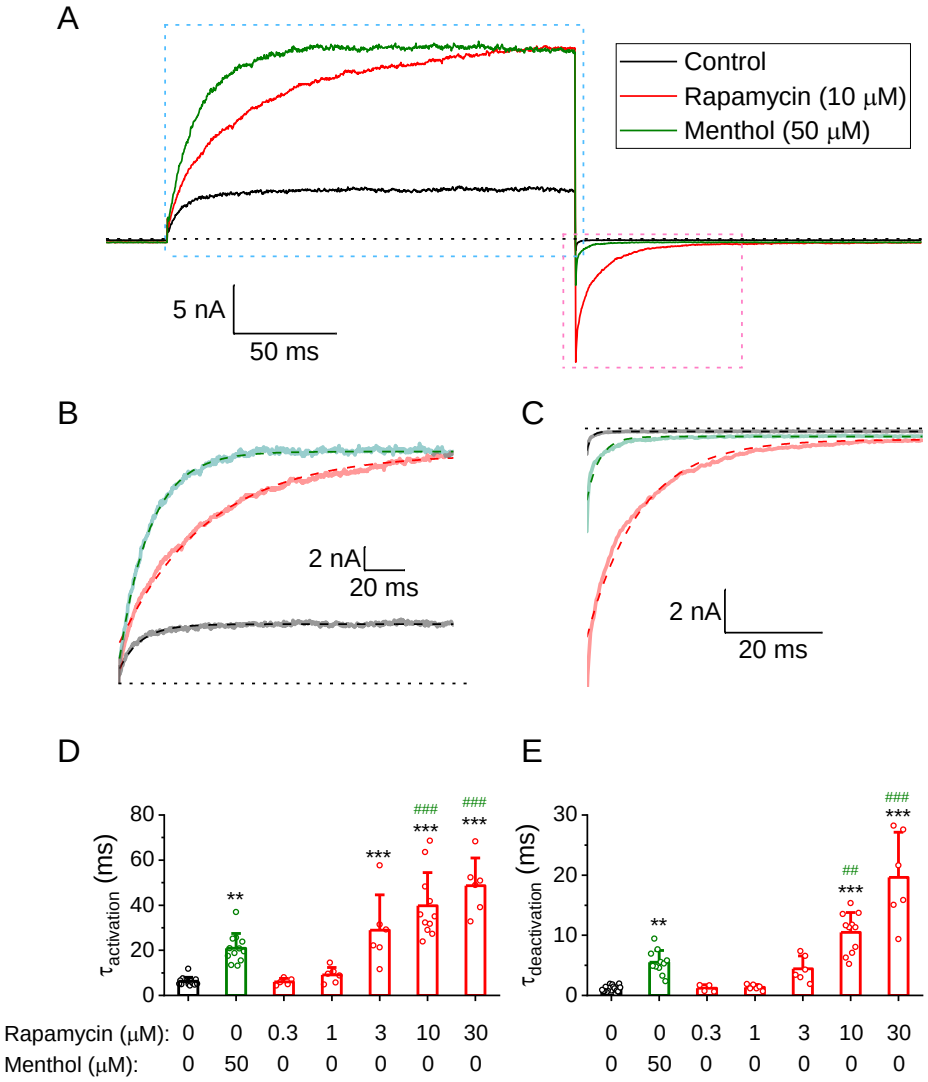

Figure S7: Rapamycin acts as a type I agonist.

(A) Representative examples of whole-cell currents in HEK293 cells expressing TRPM8, in response to a 200-ms voltage step from -80 to +120 mV and back to -80 mV, in control conditions and in the presence of the indicated concentrations of rapamycin or menthol.
(B) Zoomed-in time course of current relaxation at +120 mV. Dashed lines indicate monoexponential fits.
(C) Zoomed-in time course of current relaxation at -80 mV. Dashed lines indicate monoexponential fits.
(D) Monoexponential time constants for current activation at +120 mV in control conditions and in the presesence of the indicated concentrations of menthol or rapamycin.
(E) Monoexponential time constants for current deactivation at -80 mV in control conditions and in the presesence of the indicated concentrations of menthol or rapamycin. **, ***:

P<0.01, P<0.001 *versus* control. ##, ###: P<0.01, P<0.001 *versus* menthol. Mean ± SD, dots represent individual cases.

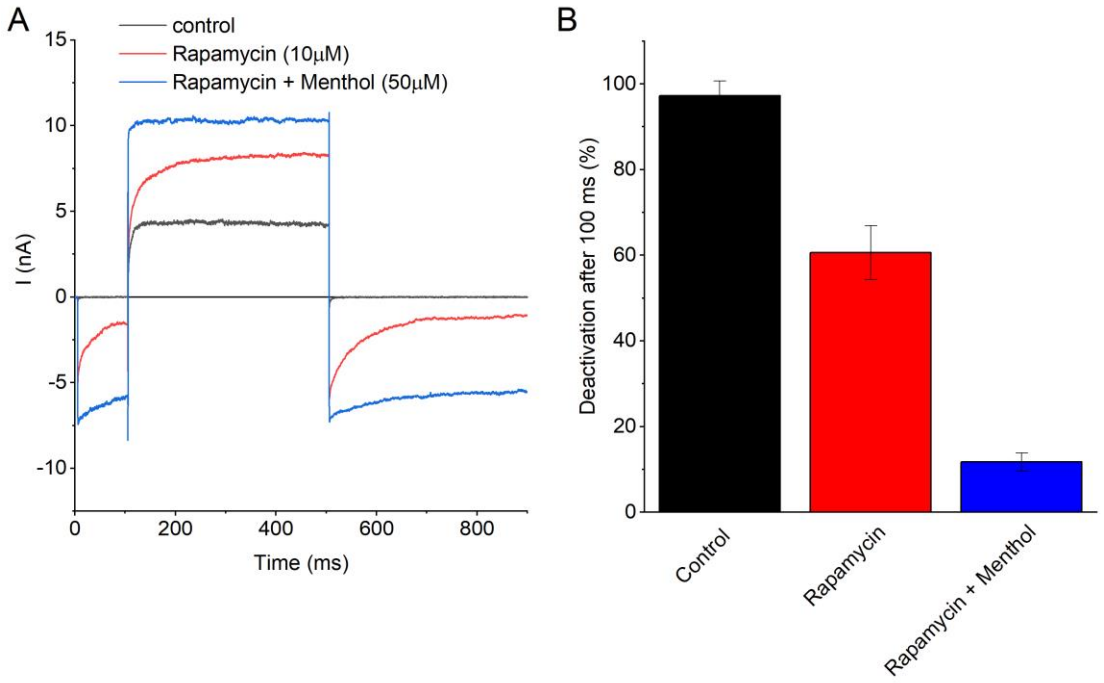

Figure S8: Additive effects of Rapamycin and menthol and TRPM8 deactivation.

(A) Representative examples of whole-cell currents in HEK293 cells expressing TRPM8, in response to a 200-ms voltage step from -120 to +120 mV and back to -120 mV, in control conditions, in the presence of rapamycin (10 μM) and in the combined presence of rapamycin (10 μM) and menthol (50 μM).

(B) Mean current deactivation, calculated as the fraction of the peak current upon the final step to -120 mV that deactivated after 100ms. Data from N=6 cells.

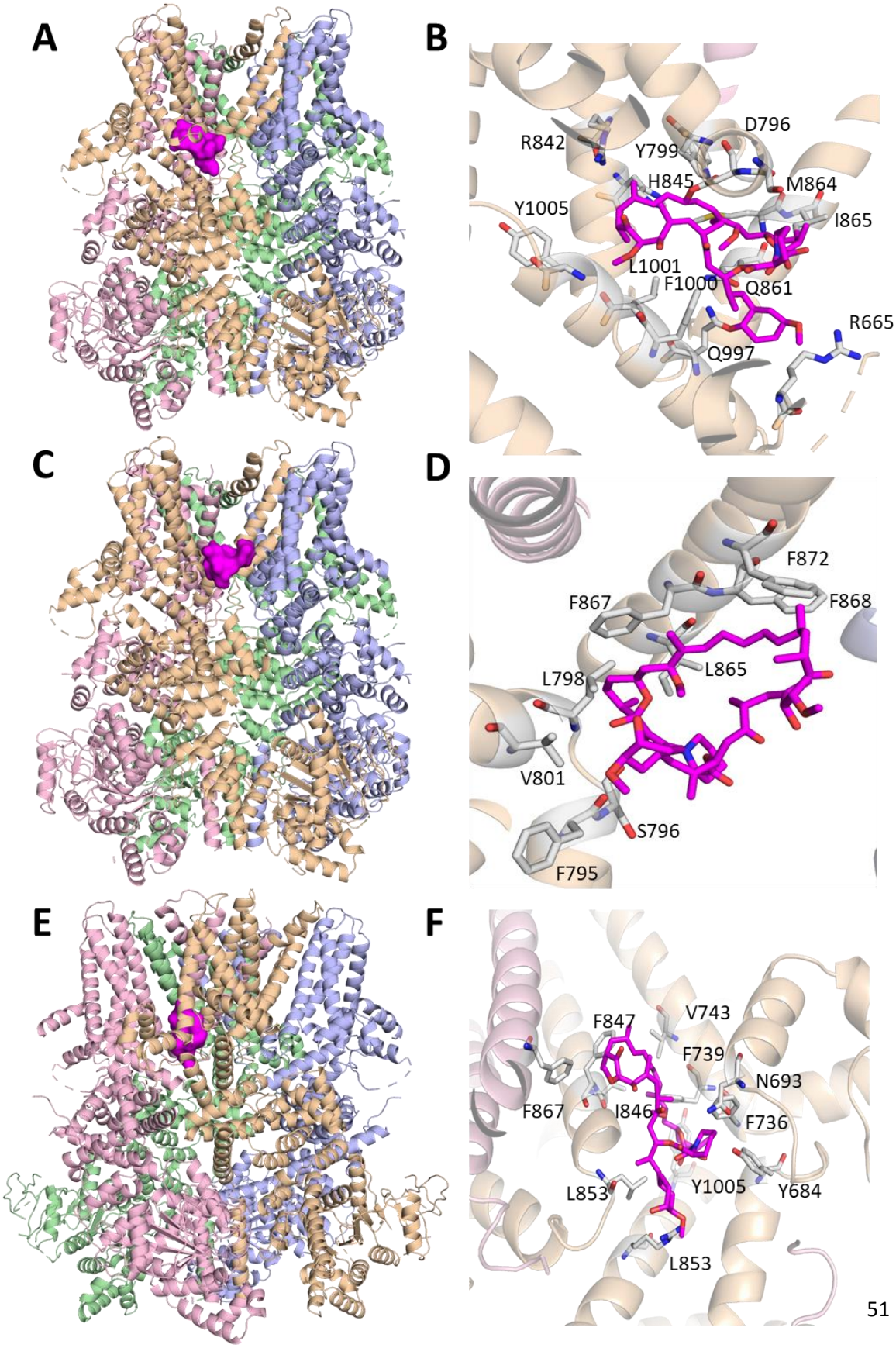
A
B
R842
D796
Y799
H845
M864
Y1005
I865
L1001
F1000
Q861
R665
Q997
C
D
F872
F867
F868
L798
L865
V801
S796
F795
E
F
F847
V743
F739
N693
F867
I846
F736
L853
Y1005
Y684
L853

Figure S9. Potential binding sites and poses of rapamycin on TRPM8 obtained from blind pilot dockings.

(A-B) site 1, (C-D) site 2, (E-F) site 3. Rapamycin was docked onto the structure of full-length TRPM8 from the collared flycatcher (*Ficedula albicollis*; pdb code: 6NR2). For clarity, the amino acid numbering refers to the corresponding residues in the human TRPM8 ortholog.

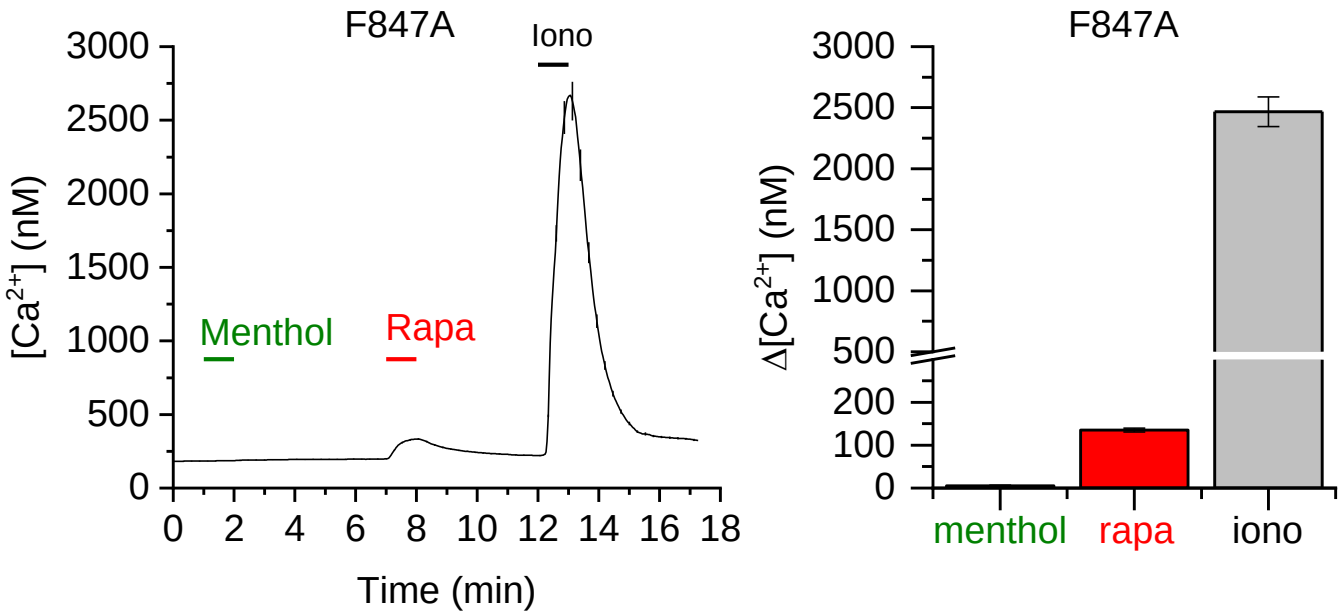

Figure S10 Rapamycin, but not menthol, moderately activates HEK cells expressing TRPM8^{F847A}

(A) Time course of the intracellular calcium concentration in HEK293 cells expressing TRPM8^{F847A}, showing moderate responses to rapamycin (10 µM) but no response to menthol (50 µM). Ionomycin was used as positive control. Shown are mean ± SEM, N=114 cells

(B) Statistical analysis on the amplitude of Ca^{2+} transients evoked by menthol (50 µM), rapamycin (10 µM) and ionomycin. Shown are mean ± SEM; N=114 cells.

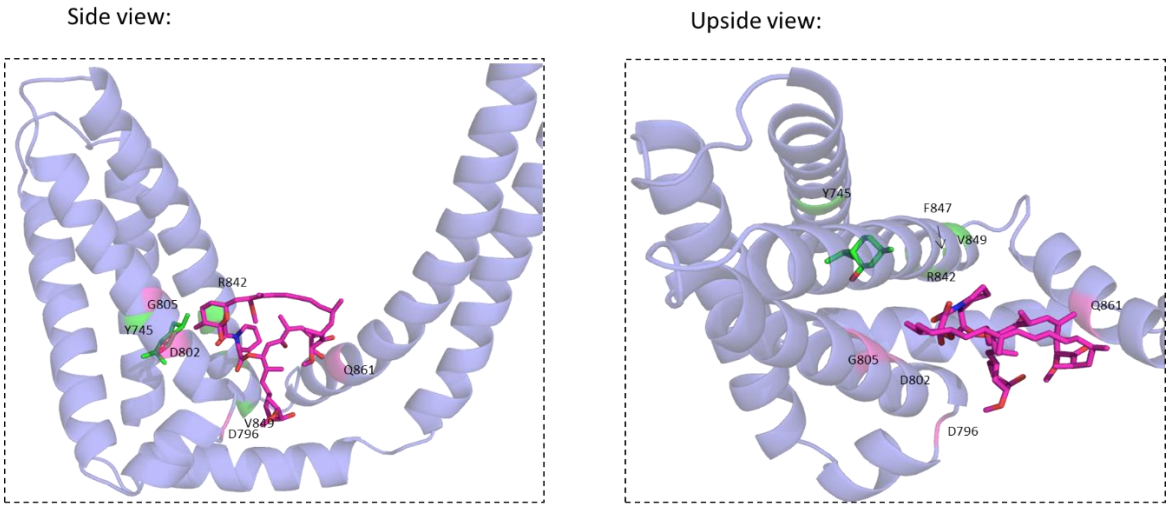

Figure S11: Structural model indicating side chains for all mutations, colored by menthol (green)/rapamycin (red) selectivity.

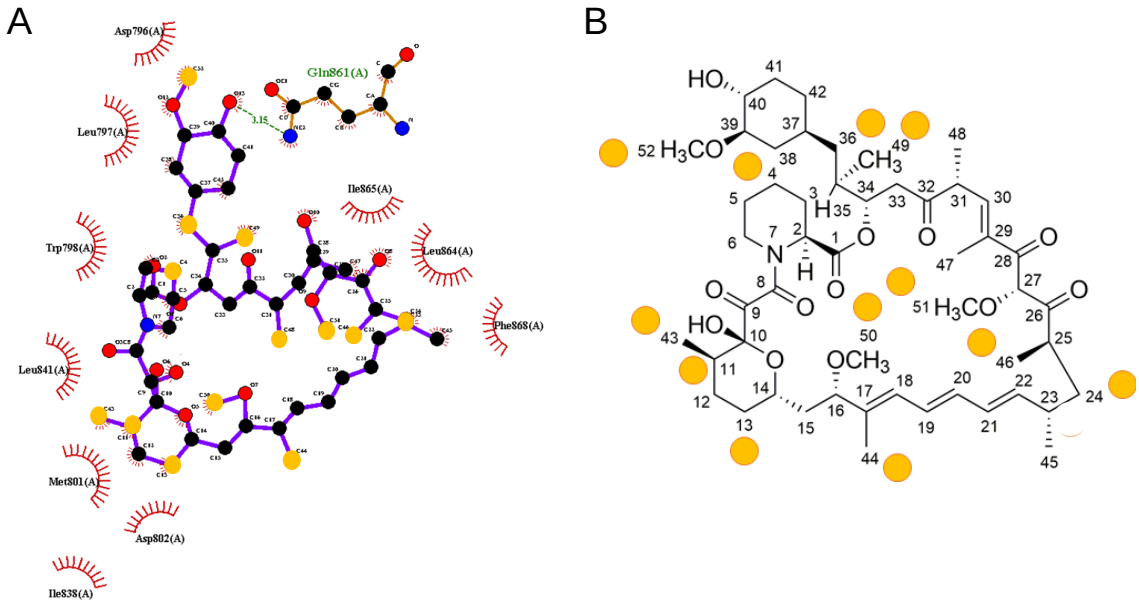

Figure S12: Visualizing and comparing the STTD NMR results with the predicted rapamycin binding pocket.

(A) 2D projection of interactions between rapamycin and TRPM8 created using Ligplot+. The yellow circles mark the carbon atoms of the rapamycin which the interacting hydrogen atoms identified by STTD NMR belong to.

(B) Structure of rapamycin indicating hydrogen atoms involved in the interaction with TRPM8. The interacting hydrogen atoms proposed by the STTD NMR experiments are marked by the yellow circles.

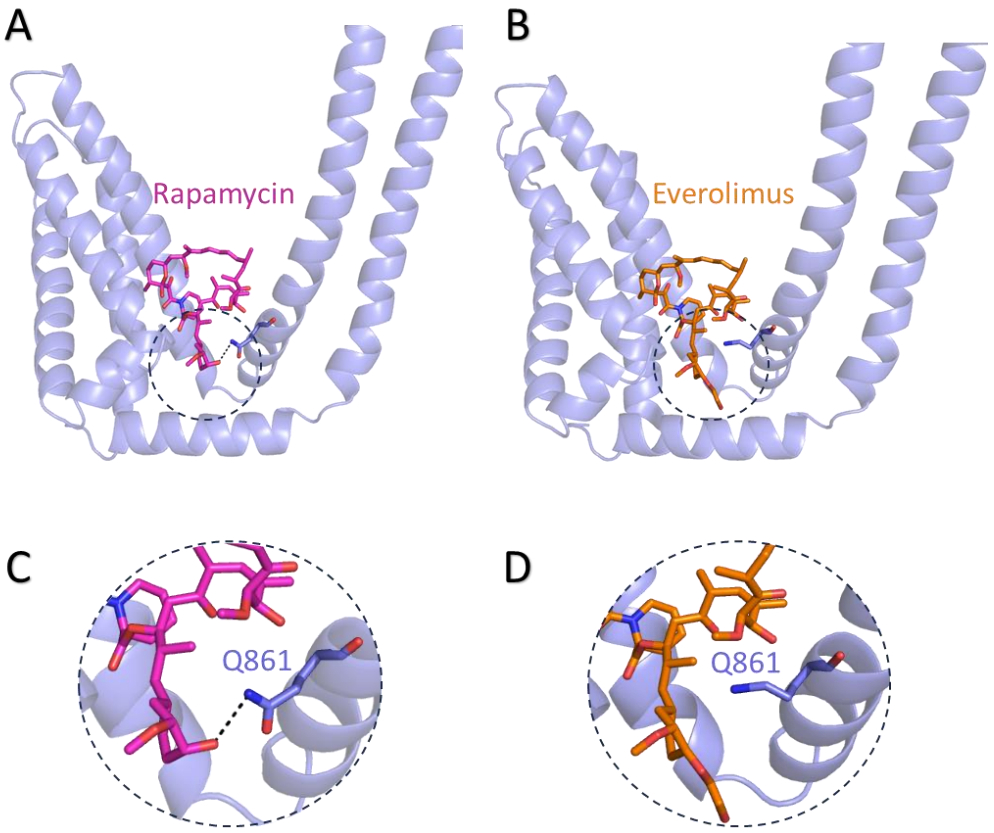

Figure S13. Molecular docking of rapamycin and everolimus to the groove between voltage sensor-like domain and the pore domain of TRPM8.

(A-B) In silico molecular docking indicates that everolimus binds to TRPM8 in a similar pose as rapamycin, albeit with lower binding energy (-8.5 kcal/mol for everolimus versus -11.6 kcal/mol for rapamycin).

(C-D) A zoom-in on the binding site shows the hydrogen bond between the hydroxyl group on the cyclohexane ring in rapamycin (C) and the side-chain amide of residue Gln861, whereas no such a hydrogen bond can be formed between the longer hydroxyethyl moiety on everolimus (D).

REFERENCES

Abraham, R. T., & Wiederrecht, G. J. (1996). Immunopharmacology of rapamycin. *Annu Rev Immunol*, *14*, 483-510. https://doi.org/10.1146/annurev.immunol.14.1.483

Aitken, P., Stanescu, I., Boddington, L., Mahon, C., Fogarasi, A., Liao, Y. H., Ivars, M., Moreno-Artero, E., Trauner, D., DeRoos, S. T., Jancic, J., Nikolic, M., Balazova, P., Price, H. N., Hadzsiev, K., Riney, K., Stapleton, S., Tollefson, M. M., Bauer, D., & Atkinson, H. (2023). A novel rapamycin cream formulation improves facial angiofibromas associated with tuberous sclerosis complex: a double-blind randomized placebo-controlled trial. *Br J Dermatol*, *189*(5), 520-530. https://doi.org/10.1093/bjd/ljad243

Ali, E. S., Mitra, K., Akter, S., Ramproshad, S., Mondal, B., Khan, I. N., Islam, M. T., Sharifi-Rad, J., Calina, D., & Cho, W. C. (2022). Recent advances and limitations of mTOR inhibitors in the treatment of cancer. *Cancer Cell Int*, *22*(1), 284. https://doi.org/10.1186/s12935-022-02706-8

Arcas, J. M., Gonzalez, A., Gers-Barlag, K., Gonzalez-Gonzalez, O., Bech, F., Demirkhanyan, L., Zakharian, E., Belmonte, C., Gomis, A., & Viana, F. (2019). The Immunosuppressant Macrolide Tacrolimus Activates Cold-Sensing TRPM8 Channels. *J Neurosci*, *39*(6), 949-969. https://doi.org/10.1523/JNEUROSCI.1726-18.2018

Bamps, D., Vriens, J., de Hoon, J., & Voets, T. (2021). TRP Channel Cooperation for Nociception: Therapeutic Opportunities. *Annu Rev Pharmacol Toxicol*, *61*, 655-677. https://doi.org/10.1146/annurev-pharmtox-010919-023238

Bandell, M., Dubin, A. E., Petrus, M. J., Orth, A., Mathur, J., Hwang, S. W., & Patapoutian, A. (2006). High-throughput random mutagenesis screen reveals TRPM8 residues specifically required for activation by menthol. *Nat Neurosci*, *9*(4), 493-500. https://doi.org/10.1038/nn1665

Bautista, D. M., Siemens, J., Glazer, J. M., Tsuruda, P. R., Basbaum, A. I., Stucky, C. L., Jordt, S. E., & Julius, D. (2007). The menthol receptor TRPM8 is the principal detector of environmental cold. *Nature*, *448*(7150), 204-208. https://doi.org/10.1038/nature05910

Beccari AR, Gemei M, Lo Monte M, Menegatti N, Fanton M, Pedretti A, Bovolenta S, Nucci C, Molteni A, Rossignoli A, Brandolini L, Taddei A, Za L, Liberati C, Vistoli G. 2017. Novel selective, potent naphthyl TRPM8 antagonists identified through a combined ligand- and structure-based virtual screening approach. *Sci Rep 7*, 10999. https://doi.org/10.1038/s41598-017-11194-0

Cao, E., Liao, M., Cheng, Y., & Julius, D. (2013). TRPV1 structures in distinct conformations reveal activation mechanisms. *Nature 504,*(7478), 113-118. https://doi.org/10.1038/nature12823

Chen, Y., & Zhou, X. (2020). Research progress of mTOR inhibitors. *Eur J Med Chem*, *208*, 112820. https://doi.org/10.1016/j.ejmech.2020.112820

Chuang, H. H., Neuhausser, W. M., & Julius, D. (2004). The super-cooling agent icilin reveals a mechanism of coincidence detection by a temperature-sensitive TRP channel. *Neuron*, *43*(6), 859-869. https://doi.org/10.1016/j.neuron.2004.08.038

Claasen, B., Axmann, M., Meinecke, R., & Meyer, B. (2005). Direct observation of ligand binding to membrane proteins in living cells by a saturation transfer double difference (STDD) NMR spectroscopy method shows a significantly higher affinity of integrin alpha(IIb)beta3

in native platelets than in liposomes. *J Am Chem Soc*, *127*(3), 916-919. https://doi.org/10.1021/ja044434w

Colburn, R. W., Lubin, M. L., Stone, D. J., Jr., Wang, Y., Lawrence, D., D'Andrea, M. R., Brandt, M. R., Liu, Y., Flores, C. M., & Qin, N. (2007). Attenuated cold sensitivity in TRPM8 null mice. *Neuron*, *54*(3), 379-386. https://doi.org/10.1016/j.neuron.2007.04.017

Dhaka, A., Murray, A. N., Mathur, J., Earley, T. J., Petrus, M. J., & Patapoutian, A. (2007). TRPM8 is required for cold sensation in mice. *Neuron*, *54*(3), 371-378. https://doi.org/10.1016/j.neuron.2007.02.024

Diver, M. M., Cheng, Y., & Julius, D. (2019). Structural insights into TRPM8 inhibition and desensitization. *Science*, *365*(6460), 1434-1440. https://doi.org/10.1126/science.aax6672

Huffer, K. E., Aleksandrova, A. A., Jara-Oseguera, A., Forrest, L. R., & Swartz, K., J. (2020). Global alignment and assessment of TRP channel transmembrane domain structures to explore functional mechanisms. *Elife, 9.* https://doi.org/10.7554/eLife.58660

Hughes, T. E., Del Rosario, J. S., Kapoor, A., Yazici, A. T., Yudin, Y., Fluck, E. C., Filizola, M., Rohacs, T., & Moiseenkova-Bell V. Y. (2019). Structure-based characterization of novel TRPV5 inhibitors. *Elife 8*. https://doi.org/10.7554/eLife.49572

Iftinca, M., & Altier, C. (2020). The cool things to know about TRPM8! *Channels (Austin)*, *14*(1), 413-420. https://doi.org/10.1080/19336950.2020.1841419

Janssens, A., Gees, M., Toth, B. I., Ghosh, D., Mulier, M., Vennekens, R., Vriens, J., Talavera, K., & Voets, T. (2016). Definition of two agonist types at the mammalian cold-activated channel TRPM8. *Elife*, *5*. https://doi.org/10.7554/eLife.17240

Jimeno, A., Rudek, M. A., Kulesza, P., Ma, W. W., Wheelhouse, J., Howard, A., Khan, Y., Zhao, M., Jacene, H., Messersmith, W. A., Laheru, D., Donehower, R. C., Garrett-Mayer, E., Baker, S. D., & Hidalgo, M. (2008). Pharmacodynamic-guided modified continuous reassessment method-based, dose-finding study of rapamycin in adult patients with solid tumors. *J Clin Oncol*, *26*(25), 4172-4179. https://doi.org/10.1200/JCO.2008.16.2347

Karashima, Y., Damann, N., Prenen, J., Talavera, K., Segal, A., Voets, T., & Nilius, B. (2007). Bimodal action of menthol on the transient receptor potential channel TRPA1. *J Neurosci*, *27*(37), 9874-9884. https://doi.org/10.1523/JNEUROSCI.2221-07.2007

Kashio, M., & Tominaga, M. (2022). TRP channels in thermosensation. *Curr Opin Neurobiol*, *75*, 102591. https://doi.org/10.1016/j.conb.2022.102591

Kelemen, B., Pinto, S., Kim, N., Lisztes, E., Hanyicska, M., Vladar, A., Olah, A., Penzes, Z., Shu, B., Vriens, J., Biro, T., Rohacs, T., Voets, T., & Toth, B. I. (2021). The TRPM3 ion channel mediates nociception but not itch evoked by endogenous pruritogenic mediators. *Biochem Pharmacol*, *183*, 114310. https://doi.org/10.1016/j.bcp.2020.114310

Kwon, D. H., Zhang, F., Suo, Y., Bouvette, J., Borgnia, M. J., & Lee, S. (2021). Heat-dependent opening of TRPV1 in the presence of capsaicin. *Nat Struct Mol Biol, 28*(7), 554-563. https://doi.org/10.1038/s41594-021-00616-3

Lamming, D. W., Ye, L., Sabatini, D. M., & Baur, J. A. (2013). Rapalogs and mTOR inhibitors as anti-aging therapeutics. *J Clin Invest*, *123*(3), 980-989. https://doi.org/10.1172/JCI64099

Lashinger, E. S., Steiginga, M. S., Hieble, J. P., Leon, L. A., Gardner, S. D., Nagilla, R., Davenport, E. A., Hoffman, B. E., Laping, N. J., & Su, X. (2008). AMTB, a TRPM8 channel blocker: evidence in rats for activity in overactive bladder and painful bladder syndrome. *Am J Physiol Renal Physiol*, *295*(3), F803-810. https://doi.org/10.1152/ajprenal.90269.2008

Liu, B., Fan, L., Balakrishna, S., Sui, A., Morris, J. B., & Jordt, S. E. (2013). TRPM8 is the principal mediator of menthol-induced analgesia of acute and inflammatory pain. *Pain*, *154*(10), 2169-2177. https://doi.org/10.1016/j.pain.2013.06.043

Mahieu, F., Janssens, A., Gees, M., Talavera, K., Nilius, B., & Voets, T. (2010). Modulation of the cold-activated cation channel TRPM8 by surface charge screening. *J Physiol*, *588*(Pt 2), 315-324. https://doi.org/10.1113/jphysiol.2009.183582

Malkia A, Pertusa M, Fernández-Ballester G, Ferrer-Montiel A, Viana F. 2009. Differential Role of the Menthol-Binding Residue Y745 in the Antagonism of Thermally Gated TRPM8 Channels. *Mol Pain 5,* 1744-8069-5–62. https://doi.org/10.1186/1744-8069-5-62

McCormack, F. X., Inoue, Y., Moss, J., Singer, L. G., Strange, C., Nakata, K., Barker, A. F., Chapman, J. T., Brantly, M. L., Stocks, J. M., Brown, K. K., Lynch, J. P., 3rd, Goldberg, H. J., Young, L. R., Kinder, B. W., Downey, G. P., Sullivan, E. J., Colby, T. V., McKay, R. T., . . . Group, M. T. (2011). Efficacy and safety of sirolimus in lymphangioleiomyomatosis. *N Engl J Med*, *364*(17), 1595-1606. https://doi.org/10.1056/NEJMoa1100391

McKemy, D. D., Neuhausser, W. M., & Julius, D. (2002). Identification of a cold receptor reveals a general role for TRP channels in thermosensation. *Nature*, *416*(6876), 52-58. https://doi.org/10.1038/nature719

Meyer, B., & Peters, T. (2003). NMR spectroscopy techniques for screening and identifying ligand binding to protein receptors. *Angew Chem Int Ed Engl*, *42*(8), 864-890. https://doi.org/10.1002/anie.200390233

Morice, M. C., Serruys, P. W., Sousa, J. E., Fajadet, J., Ban Hayashi, E., Perin, M., Colombo, A., Schuler, G., Barragan, P., Guagliumi, G., Molnar, F., Falotico, R., & Lesions, R. S. G. R. S. w. t. S.-C. B. V. B.-E. S. i. t. T. o. P. w. d. N. N. C. A. (2002). A randomized comparison of a sirolimus-eluting stent with a standard stent for coronary revascularization. *N Engl J Med*, *346*(23), 1773-1780. https://doi.org/10.1056/NEJMoa012843

Muthuswamy, S. K., Gilman, M., & Brugge, J. S. (1999). Controlled dimerization of ErbB receptors provides evidence for differential signaling by homo- and heterodimers. *Mol Cell Biol*, *19*(10), 6845-6857. https://doi.org/10.1128/MCB.19.10.6845

Ochoa, S. V., Casas, Z., Albarracin, S. L., Sutachan, J. J., & Torres, Y. P. (2023). Therapeutic potential of TRPM8 channels in cancer treatment. *Front Pharmacol*, *14*, 1098448. https://doi.org/10.3389/fphar.2023.1098448

Ormerod, A. D., Shah, S. A., Copeland, P., Omar, G., & Winfield, A. (2005). Treatment of psoriasis with topical sirolimus: preclinical development and a randomized, double-blind trial. *Br J Dermatol*, *152*(4), 758-764. https://doi.org/10.1111/j.1365-2133.2005.06438.x

Palchevskyi S, Czarnocki-Cieciura M, Vistoli G, Gervasoni S, Nowak E, Beccari AR, Nowotny M, Talarico C. 2023. Structure of human TRPM8 channel. *Commun Biol, 6,* 1–11. https://doi.org/10.1038/s42003-023-05425-6

Palkar, R., Ongun, S., Catich, E., Li, N., Borad, N., Sarkisian, A., & McKemy, D. D. (2018). Cooling Relief of Acute and Chronic Itch Requires TRPM8 Channels and Neurons. *J Invest Dermatol*, *138*(6), 1391-1399. https://doi.org/10.1016/j.jid.2017.12.025 Paricio-Montesinos, R., Schwaller, F., Udhayachandran, A., Rau, F., Walcher, J., Evangelista, R., Vriens, J., Voets, T., Poulet, J. F. A., & Lewin, G. R. (2020). The Sensory Coding of Warm Perception. *Neuron*, *106*(5), 830-841 e833. https://doi.org/10.1016/j.neuron.2020.02.035

Peier, A. M., Moqrich, A., Hergarden, A. C., Reeve, A. J., Andersson, D. A., Story, G. M., Earley, T. J., Dragoni, I., McIntyre, P., Bevan, S., & Patapoutian, A. (2002). A TRP channel that senses

cold stimuli and menthol. *Cell*, *108*(5), 705-715. https://doi.org/10.1016/s0092-8674(02)00652-9

Plaza-Cayón A, González-Muñiz R, Martín-Martínez M. 2022. Mutations of TRPM8 channels: Unraveling the molecular basis of activation by cold and ligands. *Medicinal Research Reviews 42*, 2168–2203. https://doi.org/10.1002/med.21920

Rohacs, T., Lopes, C. M., Michailidis, I., & Logothetis, D. E. (2005). PI(4,5)P2 regulates the activation and desensitization of TRPM8 channels through the TRP domain. *Nat Neurosci*, *8*(5), 626-634. https://doi.org/10.1038/nn1451

Selvarani, R., Mohammed, S., & Richardson, A. (2021). Effect of rapamycin on aging and age-related diseases-past and future. *Geroscience*, *43*(3), 1135-1158. https://doi.org/10.1007/s11357-020-00274-1

Soria, A., Agbo-Godeau, S., Taieb, A., & Frances, C. (2009). Treatment of refractory oral erosive lichen planus with topical rapamycin: 7 cases. *Dermatology*, *218*(1), 22-25. https://doi.org/10.1159/000172830

Suh, B. C., Inoue, T., Meyer, T., & Hille, B. (2006). Rapid chemically induced changes of PtdIns(4,5)P2 gate KCNQ ion channels. *Science*, *314*(5804), 1454-1457. https://doi.org/10.1126/science.1131163

Swarbrick, A. W., Frederiks, A. J., & Foster, R. S. (2021). Systematic review of sirolimus in dermatological conditions. *Australas J Dermatol*, *62*(4), 461-469. https://doi.org/10.1111/ajd.13671

Trepanier, D. J., Gallant, H., Legatt, D. F., & Yatscoff, R. W. (1998). Rapamycin: distribution, pharmacokinetics and therapeutic range investigations: an update. *Clin Biochem*, *31*(5), 345-351. https://doi.org/10.1016/s0009-9120(98)00048-4

Vandewauw, I., De Clercq, K., Mulier, M., Held, K., Pinto, S., Van Ranst, N., Segal, A., Voet, T., Vennekens, R., Zimmermann, K., Vriens, J., & Voets, T. (2018). A TRP channel trio mediates acute noxious heat sensing. *Nature*, *555*(7698), 662-666. https://doi.org/10.1038/nature26137

Varnai, P., Thyagarajan, B., Rohacs, T., & Balla, T. (2006). Rapidly inducible changes in phosphatidylinositol 4,5-bisphosphate levels influence multiple regulatory functions of the lipid in intact living cells. *J Cell Biol*, *175*(3), 377-382. https://doi.org/10.1083/jcb.200607116

Vezina, C., Kudelski, A., & Sehgal, S. N. (1975). Rapamycin (AY-22,989), a new antifungal antibiotic. I. Taxonomy of the producing streptomycete and isolation of the active principle. *J Antibiot (Tokyo)*, *28*(10), 721-726. https://doi.org/10.7164/antibiotics.28.721

Voets, T., Droogmans, G., Wissenbach, U., Janssens, A., Flockerzi, V., & Nilius, B. (2004). The principle of temperature-dependent gating in cold- and heat-sensitive TRP channels. *Nature*, *430*(7001), 748-754. https://doi.org/10.1038/nature02732

Voets, T., Owsianik, G., Janssens, A., Talavera, K., & Nilius, B. (2007). TRPM8 voltage sensor mutants reveal a mechanism for integrating thermal and chemical stimuli. *Nat Chem Biol*, *3*(3), 174-182. https://doi.org/10.1038/nchembio862

Vriens, J., Nilius, B., & Voets, T. (2014). Peripheral thermosensation in mammals. *Nat Rev Neurosci*, *15*(9), 573-589. https://doi.org/10.1038/nrn3784

Winstein, S., & Henderson, R. B. (1943). The Role of Neighboring Groups in Replacement Reactions. VII. The Methoxyl Group. *J. Am. Chem. Soc.* , *65*, 2196–2200.

Xiao, B., Dubin, A. E., Bursulaya, B., Viswanath, V., Jegla, T. J., & Patapoutian, A. (2008). Identification of transmembrane domain 5 as a critical molecular determinant of menthol

sensitivity in mammalian TRPA1 channels. *J Neurosci*, *28*(39), 9640-9651. https://doi.org/10.1523/JNEUROSCI.2772-08.2008

Xu, L., Han, Y., Chen, X., Aierken, A., Wen, H., Zheng, W., Wang, H., Lu, X., Zhao, Z., Ma, C., Liang, P., Yang, W., Yang, S., & Yang, F. (2020). Molecular mechanisms underlying menthol binding and activation of TRPM8 ion channel. *Nat Commun*, *11*(1), 3790. https://doi.org/10.1038/s41467-020-17582-x

Yin, Y., Le, S. C., Hsu, A. L., Borgnia, M. J., Yang, H., & Lee, S. Y. (2019). Structural basis of cooling agent and lipid sensing by the cold-activated TRPM8 channel. *Science*, *363*(6430). https://doi.org/10.1126/science.aav9334

Yin, Y., Wu, M., Zubcevic, L., Borschel, W. F., Lander, G. C., & Lee, S. Y. (2018). Structure of the cold- and menthol-sensing ion channel TRPM8. *Science*, *359*(6372), 237-241. https://doi.org/10.1126/science.aan4325

Yin, Y., Zhang, F., Feng, S., Butay, K. J., Borgnia, M. J., Im, W., & Lee, S. Y. (2022). Activation mechanism of the mouse cold-sensing TRPM8 channel by cooling agonist and PIP(2). *Science*, *378*(6616), eadd1268. https://doi.org/10.1126/science.add1268

Zhang, X., Chen, W., Gao, Q., Yang, J., Yan, X., Zhao, H., Su, L., Yang, M., Gao, C., Yao, Y., Inoki, K., Li, D., Shao, R., Wang, S., Sahoo, N., Kudo, F., Eguchi, T., Ruan, B., & Xu, H. (2019), Rapamycin directly activates lysosomal mucolipin TRP channels independent of mTOR. *PLoS Biol, 17*(5), e3000252. https://doi.org/10.1371/journal.pbio.3000252

Zhao, C., Xie, Y., Xu, L., Ye, F., Xu, X., Yang, W., Yang, F., & Guo, J. (2022). Structures of a mammalian TRPM8 in closed state. *Nat Commun*, *13*(1), 3113. https://doi.org/10.1038/s41467-022-30919-y